UCLouvain

epl

École polytechnique de Louvain

Poly(lactic acid)/poly(ethylene glycol) blends for the production of porous scaffold biomaterials

Author: **Leila MATHOT**
Supervisors: **Sophie DEMOUSTIER, Alain JONAS**
Readers: **Quentin PAPELOER, Evelyne VAN RUYMBEKE**
Academic year 2022–2023
Master [120] in Biomedical Engineering

Abstract

Tissue engineering is a promising field that aims to repair or replace damaged tissues. Tissue engineering requires the production of porous scaffold biomaterials, exhibiting both micro- and macroporosity. In this study, we created polymer blends and induced microporosity in these blends. Poly(lactic acid) (PLA) was blended with poly(ethylene glycol) (PEG); the blends were first melted, then subjected to crystallization along with liquid-solid phase separation between PEG and PLA, leading to PEG rich regions within PLA, and the PEG phase was extracted to create pores in the samples. Two parameters were studied to optimize the pore size and distribution: PEG molar mass, and PEG content in the blend. The porosity was studied using polarized-light optical microscopy (POM), scanning electron microscopy (SEM), and confocal laser scanning microscopy (CLSM).

Both PEG content and PEG molar mass proved to have an influence on blend porosity. All blends exhibit inter- as well as intraspherulitic porosity. Blends made with a smaller amount of PEG with higher molar masses show interspherulitic porosity as well as interfibrillar porosity, within the spherulites. Indeed, during PLA crystallization, PEG diffuses outwards from PLA spherulites but some PEG is trapped within the growing PLA spherulites, in interfibrillar regions. When the PEG is extracted, pores remain in the regions where PEG was located. Pore sizes vary from a few tens of nanometers to 5 μm, allowing nutrients and cells to diffuse through the scaffold. However, when the PEG content is too high, large quantities of PEG accumulate in interspherulitic regions and large holes remain in these regions after PEG extraction; the samples are therefore brittle. When PEG molar mass is too low, PEG diffuses at a faster rate outside the growing PLA spherulites during crystallization, large amounts of PEG segregate in interpherulitic regions and larger pores are present in interspherulitic regions after PEG extraction, making the sample too brittle as well.

According to the obtained results, PLA/PEG blends with PEG extraction can be an appropriate candidate for use in tissue engineering applications. The content of PEG in the blend and its molar mass must be carefully chosen. However, many aspects of the scaffold remain to be studied, such as mechanical properties, degradability and biocompatibility.

Acknowledgements

First of all, I would like to thank my supervisors: Prof. Alain Jonas and Prof. Sophie Demoustier-Champagne for their help, for the time they devoted to me and for their explanations and sound advice.

I would like to thank Quentin Papeloer for his help and his support throughout my work. He devoted a lot of time to me as well, he showed me the different instruments in the lab, and guided me through this thesis.

I also thank Delphine Magnin for explaining and showing me how to use the SEM, Colette Douchamps for making microtome sections of my samples, and Marie-Christine Eloy for imaging the samples with me using confocal microscopy.

I thank UCLouvain for providing me with the equipment I needed for my various experiments, for allowing me to spend five years studying within the university, and for giving me the chance to go on an exchange.

Finally, I would like to thank my family and my friends for supporting me throughout my studies and thesis.

Acronyms

ABS Acrylonitrile butadiene styrene.

CCD Charge Coupled Device.

CLSM Confocal Laser Scanning Microscopy.

CT Computed Tomography.

ECM Extracellular matrix.

FDA Food and Drug Administration.

FDM Fused Deposition Modeling.

GS Gentamicin sulphate.

LA Lactic acid.

LM Low Magnification.

$\mathbf{M}_n$ Number-average molar mass.

MM Molar Mass.

mPEG methoxy poly(ethylene glycol).

MSC Mesenchymal Stem Cell.

PA Polyamide.

PBS Phosphate Buffered Saline.

PC Polycarbonate.

PCL Polycaprolactone.

PDLA Poly(D-lactic acid).

PDLLA Poly(D,L-lactic acid).

PE Poly(ethylene).

PEG Poly(ethylene glycol).

PEO Poly(ethylene oxide).

PLA Poly(lactic acid).

PLLA Poly(L-lactic acid).

POM Polarized Optical Microscopy.

PP Poly(propylene).

RM Regenerative Medicine.

ROP Ring Opening Polymerization.

rpm revolutions per minute.

SBF Simulated Body Fluid.

SEI Secondary Electron Imaging.

SEM Scanning Electron Microscopy.

SLA Stereolithography apparatus.

SLS Selective Laser Sintering.

$\mathbf{T}_c$ Crystallization temperature.

$\mathbf{T}_g$ Glass transition temperature.

$\mathbf{T}_m$ Melting temperature.

TE Tissue Engineering.

Contents

1 Introduction **1**

2 State of the Art **4**
2.1 PLA 4
2.1.1 Overview 4
2.1.2 Properties 6
2.1.3 Crystallization 8
2.1.4 Limitations 12
2.1.5 Biomedical applications 12
2.2 PLA/PEG blends 15
2.2.1 PEG properties 15
2.2.2 Crystallization 16
2.2.3 Degradation rate 19
2.2.4 Mechanical properties 19
2.2.5 Biomedical applications 19
2.3 The importance of porosity in scaffolds 21
2.3.1 Overview 21
2.3.2 Porous scaffolds fabrication techniques 21
2.3.3 Porosity of PLA-based scaffolds 25
2.3.4 Porosity of PLA/PEG scaffolds 26

3 Objectives and Strategy **31**
3.1 Objectives 31
3.2 Strategy 33

4 Materials and methods **35**
4.1 Materials 35
4.2 Films preparation 35
4.3 Isothermal crystallization 36
4.4 Extraction method 37
4.5 Sections of the samples 37

4.6 Characterization techniques 37
4.6.1 Polarized-light optical microscopy 37
4.6.2 Scanning electron microscopy 38
4.6.3 Confocal laser scanning microscopy 38

5 Results and discussion **39**
5.1 PEG localization after blend crystallization 40
5.2 Effect of PEG concentration 43
5.2.1 Morphology of the blends 43
5.2.2 Porosity of the blends 45
5.3 Effect of PEG molar mass 50
5.3.1 Morphology of the blends 50
5.3.2 Porosity of the blends 51
5.3.3 Morphology and porosity at different depths inside the material 56
5.4 General discussion 60

6 Conclusion **64**

Chapter 1

Introduction

One of the major current healthcare problems is tissue and organ failure as a result of disease, injury, or developmental defects [1]. Several solutions exist to treat this problem. First, tissue can be transplanted from one site of the patient to another (autograft). Unfortunately, autografts are expensive, painful and constrained by anatomical limitations [2]. Another medical alternative to treat tissue and organ failure is the use of donated tissues and organs from another individual (transplant or allograft). However, this solution faces many limitations such as the shortage of organ donors, the increasing number of people in the need of a transplantation, and an ever-increasing aging population. Due to severe logistical constraints, many organs from donors cannot be matched, transported, and successfully transplanted into a patient within the very limited time available [1]. In addition, once the tissue or organ has been implanted into the host, their immune system could reject the foreign tissue. Finally, infection or disease could be transmitted from the donor to the patient [2].

A very promising solution to address this critical medical need is the use of tissue-engineered products. Tissue engineering (TE) and regenerative medicine (RM) are multidisciplinary fields that combine knowledge and technologies from different fields such as biology, chemistry, engineering, medicine, pharmaceutical, and material science to develop therapies and products for repair or replacement of damaged tissues and organs [1]. To do so, highly porous 3D scaffold biomaterials are used to provide the appropriate environment for the regeneration of tissues and organs. Cells are seeded on the scaffold along with growth factors to induce formation and growth of new tissue. These cell-seeded scaffolds can either be cultured *in vitro* to synthesize tissues before being implanted in the patient or *in vivo*, meaning that the scaffold is directly implanted into the patient where tissues and organs will regenerate [2].

Many different scaffolds, made by several techniques and with several biomateri-

als, were already studied. A good scaffold should be biocompatible so that it is not rejected by the body when it is implanted, it should present mechanical properties similar to the ones of the tissue it is replacing, and it should have an interconnected pore structure and high porosity to ensure cellular penetration and adequate diffusion of nutrients to cells [2]. Moreover, a scaffold should be biodegradable. Indeed, several problems can be associated with long-term implants such as infection, fibrous tissue formation, and the possible need for retrieval, adding a surgical operation. The degradation rate is then optimized to allow transplanted cells to proliferate and secrete their own extracellular matrix (ECM) while the scaffold can degrade to leave enough space for new tissue growth. After a certain period of time, depending on the tissue that is replaced and its regeneration rate, only tissue created by the patient should remain. To meet these properties, polymers are widely used as scaffold biomaterials. The biodegradability of a polymer is influenced by its composition, its molar mass and molar mass distribution, and its degree of crystallinity. The environmental conditions such as temperature and pH, as well as the mechanical loading that the scaffold undergoes, also play an important role in polymer degradation [3].

There are many different techniques to fabricate 3D porous scaffolds based on polymers such as freeze-drying, electrospinning, gas foaming, 3D-printing, etc. Among 3D-printing techniques, fused deposition modeling (FDM) has been increasingly used because it is easy to use, simple to operate and it presents low cost in use and maintenance. Moreover, 3D-printing allows to design and fabricate scaffolds with a well-defined structure and larger-scale porosity (≥ 50 μm).

Poly(lactic acid) (PLA) is a synthetic polymer that is widely used as biomaterial. Indeed, this polymer is nontoxic and biocompatible. It is approved by the Food and Drug Administration (FDA). It presents good thermal properties and is easy to process, for example, by 3D-printing. PLA also presents good mechanical properties regarding its tensile strength and stiffness. However, PLA has a low elongation at break and impact strength. It is a hydrophobic polymer having a slow degradation rate and low crystallization rate. Moreover, PLA is not porous so to be used as scaffold, porosity should be induced, for example via a specific manufacturing technique.

Poly(ethylene glycol) (PEG) is a hydrophilic, biocompatible and biodegradable polymer. It is approved by the FDA. It is soluble in water and other solvents. It has a plasticizing effect on some other polymers such as PLA. When blended with PLA, it allows to improve PLA crystallization and degradation rate. Moreover, it has already been used as porogen in some applications: it is first blended with PLA and then the PEG is extracted by water immersion (PLA is not soluble in water) in order to induce porosity in the scaffold.

The aim of this thesis is to develop a porous biomaterial that can be 3D-printed for biomedical applications. We will study and compare PLA/PEG blends with different molar masses and different PEG concentrations. More precisely, the porosity of the different blends will be studied in depth depending on blend composition.

This thesis contains six chapters. Chapter 1 is the introduction. Chapter 2 presents a state of the art on what has already been done and what already exists in the field of PLA/PEG biomaterials, based on previous studies and articles. This chapter first presents PLA, its properties as well as its limitations and some biomedical applications that already exist. A section of this chapter focuses on PLA/PEG blends, their properties and some biomedical applications that were already investigated as well. Finally, the last section is dedicated to the importance of porosity in biomaterials. It presents some fabrication techniques as well as porous PLA-based scaffolds and porous PLA/PEG scaffolds. Chapter 3 presents the objectives of this thesis more in-depth, and the overall strategy used to achieve these objectives. Chapter 4 describes the experiments performed as well as the characterization techniques used, namely polarized-light optical microscopy (POM), scanning electron microscopy (SEM), and confocal laser scanning microscopy (CLSM). Chapter 5 describes the results obtained. A first section describes the effect of the concentration of PEG in PLA/PEG blends. A second section presents the effect of PEG molar mass based on the morphology and porosity of the blends. In both sections, POM and SEM micrographs are depicted. A last section contains a general discussion of the results previously described. Finally, Chapter 6 provides a conclusion of this work.

Chapter 2

State of the Art

2.1 PLA

2.1.1 Overview

Polyesters are often used in biomedical applications because they are biodegradable and relatively easy to synthesize [4]. Poly(lactic acid) or polylactide (PLA) is a polymer derived from lactic acid (LA) which is produced from renewable resources by fermentation of polysaccharides or sugar extracted from agricultural products such as corn starch, potato, sugar-beet, etc [5]. It is approved by the Food and Drug Administration (FDA) and it is nontoxic, meaning that it can be implanted in the human body [6].

Due to an asymmetric carbon atom, LA exists in two optically active forms, *L*- and *D*-LA, shown in Figure 2.1, and can be polymerized into pure poly(*L*-lactide) (PLLA), pure poly(*D*-lactide) (PDLA), or poly(*D*, *L*-lactide) (PDLLA). PLLA and PDLA are isotactic, meaning that materials formed only by one of these stereoisomers will be semi-crystalline. On the other hand, PDLLA is atactic and therefore, materials containing these isomers will be amorphous [4]. For biomedical applications, in order to maintain the desired properties of PLA, such as crystallinity and biodegradability, it is crucial to utilize optically pure LA without enantiomeric impurities. LA can be produced either by chemical synthesis (based on petrochemical feedstock) or by microbial fermentation routes, as shown in Figure 2.2 [6, 7]. The latter approach has many benefits, such as producing optically pure *L*- or *D*-LA, reducing the use of petrochemical resources, and presenting a lower environmental impact. A variety of microbial species, including bacteria, fungi, yeast, cyanobacteria, or algae, can be employed to produce LA. PLA synthesis necessitates the use of catalysts under strictly controlled conditions of temperature, pressure, and pH, resulting in extended polymerization times and high energy consumption [6].

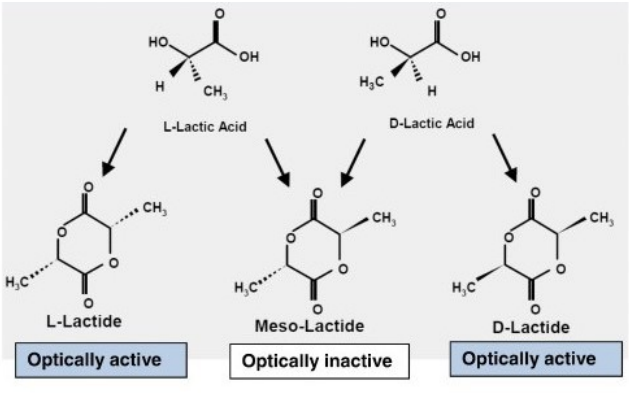

Figure 2.1: Two enantiomeric forms *L(+)-* and *D(-)-* lactic acid (LA), and their stereoisomers, taken from [8].

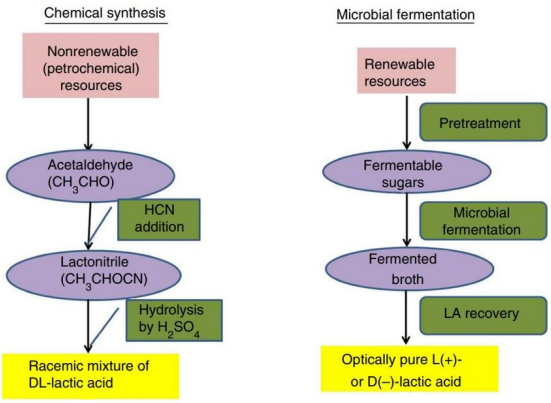

Figure 2.2: Two LA production methods: chemical and biological, adapted from [6].

The synthesis of PLA involves the processing and polymerization of LA monomer. PLA synthesis requires three steps:

- LA production by microbial fermentation;
- LA purification followed by its cyclic dimer (lactide) preparation;
- polycondensation of LA or ring opening polymerization (ROP) of lactides.

To achieve high molar mass polymers, the most commonly employed method is ring opening polymerization. This process entails the utilization of a catalyst, such as transition metals like tin, aluminium, lead, zinc, bismuth, ion, or yttrium, for the ring opening polymerization of the LA cyclic dimer [6]. Aside from polycondensation

and ROP, PLA can be synthesized by direct methods such as azeotropic dehydration and enzymatic polymerization [9]. A summary of the different methods to synthesize PLA is shown in Figure 2.3.

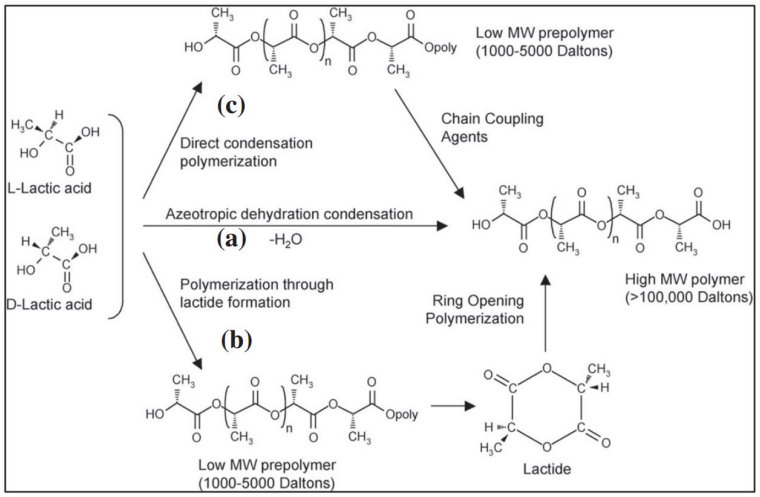

Figure 2.3: Different synthesis methods of PLA, taken from [8].

2.1.2 Properties

PLA is eco-friendly, nontoxic and presents high biocompatibility with the human body and high biodegradability, making it very promising for applications in the medical field. The properties of PLA are significantly influenced by its stereochemistry and thermal history, specifically its crystallinity [6]. With higher *D*-LA content, PLA is amorphous [7]. When the content in *L*-LA is increased above 90%, PLA becomes more crystalline in nature. The melting temperature (T_m) and the glass transition temperature (T_g) of PLA decline as the purity of PLLA decreases. PLLA is a semi-crystalline polymer with a melting point of around 170-180°C [6]. The physical characteristics of PLA, such as density (1.24 g/cm^3), heat capacity, and mechanical and rheological properties, are dependent on its crystallinity and/or transition temperatures [6, 10, 11]. PLA has a tensile modulus of about 3 GPa and a a tensile strength of about 59 MPa [12]. The complex viscosity of PLA is approximately 800 Pa×s [13]. At 25°C, its storage modulus is about 2600 MPa and at 70°C, it decreases to 100 MPa [12].

An advantage of PLA is its processability. Indeed, compared to other polymers, PLA presents good thermal processability. It can be processed by injection molding, film extrusion, blow molding, thermoforming, fiber spinning, film forming, particles leaching, solvent casting, or three-dimensional printing (3D-printing) [9, 14, 15].

As previously said, PLA can be either amorphous or semi-crystalline. Its T_m is approximately 180°C and its T_g is about 55°C. Molar mass and composition (stereoisomers content) influence PLA thermal properties such as its T_m and T_g. When the molar mass increases, T_g increases as well until it reaches a constant value [7].

The degree of crystallinity of a PLA blend can be computed according to the following formula [5]:

$$\chi_c(\%) = \frac{\Delta H_m}{\Delta H_m^0} \frac{100}{\omega}$$

with ΔH_m the melting enthalpy of the blend, ΔH_m^0 the crystallization enthalpy of PLA at which the crystallinity is 100% (equal to 93.7 J/g), and ω the mass fraction of PLA in the blend (for pure PLA, ω is equal to 1) [5].

PLLA presents a degree of crystallinity lying between 0 and 37% and has a crystallization temperature (T_c) in the range 110-130°C. As previously mentioned, PDLLA is amorphous and PDLA is semi-crystalline.

PLA is a biodegradable polymer. Various factors influence its rate of degradation. These factors can be dependent on the medium in which PLA is immersed, on the temperature and the humidity of the medium, or can be related to PLA itself, depending on its chemical parameters including molar mass and composition, PLA crystallinity, and water diffusion rate into the polymer. When implanted in the human body, PLA starts to degrade via hydrolysis of backbone ester groups that forms soluble oligomers that are then metabolized by cells [7, 9]. When PLA degrades, it releases products that, at a low concentration, are nontoxic for the human body. Indeed, during its hydrolytic degradation, PLA degrades into its monomer, i.e. lactic acid, which is produced daily in small amount by the body [16, 17]. It can be in direct contact with biological fluids such as blood, allowed by the FDA [9].

Regarding its mechanical properties, PLA presents advantages and drawbacks. In reference to other traditional polymers such as polyethylene (PE), polypropylene (PP), or polycaprolactone (PCL) which is also biocompatible, PLA exhibits good tensile strength and Young's modulus, and therefore presents a good stiffness, as shown in Table 2.1. However, it has lower elongation at break and impact strength. PLA is indeed a brittle material and presents a poor toughness, limiting its use in some applications [7].

Finally, a major disadvantage of PLA is its hydrophobicity. Hydrophobicity reduces the degradability of a tissue engineering scaffold because water cannot penetrate into the structure if the polymer is hydrophobic. Altough PLA is biodegradable, it presents a degradation rate too slow for some biomedical applications. Adhesion of cells on a biomaterial surface is very important to develop a functional tissue-engineered product. Cell adhesion is greatly influenced by the

surface hydrophilicity. Amino acids present on the outer side of the cell membrane are hydrophilic. Therefore, hydrophilic surfaces presenting a contact angle lying between 40 and 70° are more suitable for cell adhesion [18]. If adhesion of cells on the biomaterial scaffold is low, when the biomaterial is implanted into the living host body, it could induce an inflammatory response from the host upon direct contact with biological fluids [9].

Table 2.1: Mechanical properties of PLLA, PE, PP, and PCL [19–24].

	PLLA	**PE**	**PP**	**PCL**
Young's modulus [GPa]	3-7	7.2	0.54	0.34-0.36
Tensile strength [MPa]	59-66	27.4-33.4	27	23
Elongation to failure [%]	4-7	685-730	322	>700

2.1.3 Crystallization

Overview

During polymer crystallization, a high order structure, called spherulite, is created, as shown in Figure 2.4. A spherulite takes the form of a polycrystalline aggregate, itself filled with thin lamellar crystals that are made up of lamellar branches. At the nanometer scale, it can be observed that the polymer chains are arranged in a three-dimensional orthorhombic crystal lattice, exhibiting a translational periodicity in all three dimensions (Figure 2.4 (a)). The thin plate-like single crystal formed by polymeric chains exhibits characteristics such as folding at upper and lower lamellar surfaces, also known as folding surfaces. This single crystal is about 10 nm thick (Figure 2.4 (b)). By stacking lamellar crystals along with amorphous layers between them, the growth of crystals takes place (Figure 2.4 (d)) [25]. Amorphous and crystalline regions differ by their chain arrangement and density. The polymer chains are packed together in a more tight and efficient way in the crystalline domains than in the amorphous ones. The density in crystalline regions is therefore higher. Consequently, the density of a polymer increases with its degree of crystallinity χ_c [26]. The process of crystallization of polymers from the melt, concentrated solutions, or viscous liquids leads to the formation of a spherulitic structure characterized by chain-folded lamellar crystallites that radiate and fill the space. A single spherulite has a diameter depending on the nucleation density, typically about 100 μm in PLLA (Figure 2.4 (c, e, f)) [25].

Depending on the orientation of the lamellae, spherulites present two distinct inner structures. The most common orientation for PLA spherulites is random directions and is the one represented in Figure 2.4. With random directions of the lamellae, the inner structure presents patchy patterns when viewed between

crossed polarizers, as depicted in Figure 2.5 and 2.6, *right*. With correlated twisting, it is characterized by periodic concentric banding, as depicted in Figure 2.5 and 2.6, *left* [25, 27]. Thanks to this continuous spiral twisting, lamellae crystals are orderly and synchronously packed to create ring-banded spherulites [28]. The molecular-level structures such as chain conformation, packing and surface folding are responsible for the inherent torsional stress and twisting correlation, resulting in banded spherulites [27].

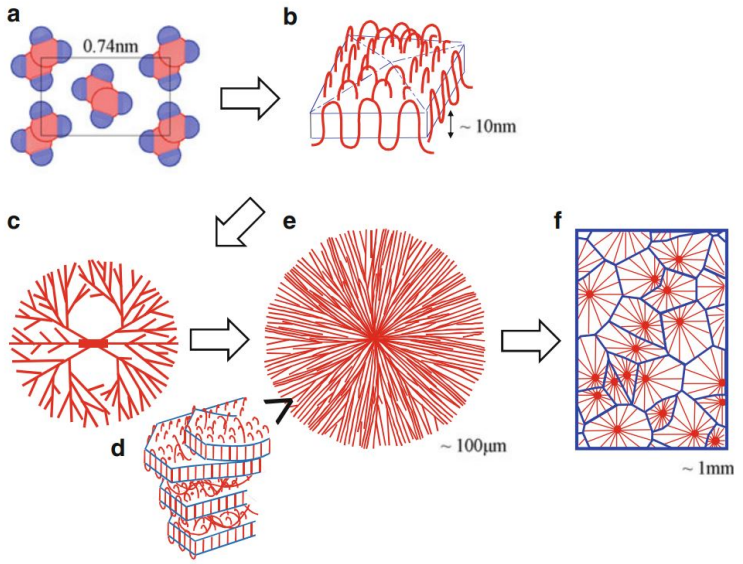

Figure 2.4: Spherulitic structure, taken from [25]. (a) Polymer chains arranged in a three-dimensional crystal lattice. (b) Thin plate-like single crystal formed by polymeric chains. (c) Nascent spherulite. (d) Stack (or fibrils) of crystals. (e) Final spherulitic structure. (f) Grown spherulites making up the crystalline structure.

PLA crystal structure

PLA has been found to exhibit various crystal forms that are dependent on the conditions, like temperature, at which crystallization occurs: α, β, γ and δ [6, 29]. They all present distinct characteristics.

The common α crystalline form is obtained from the melt in a slow cooling procedure which allows the PLA chains to adopt the conformation of lower potential energy. Due to the similarity in the crystalline structure, the δ form is also called α' or imperfect α form and is observed in samples processed from the melt with a fast cooling procedure. The crystallization of PLA at high super cooling of the melt leads to the formation of the disordered conformation, i.e., α' crystals [29]. Below

110°C, the α' crystals usually occurs. At temperature higher than 110°C, both α and α' phases coexist. If the temperature is even higher, we only observe the α form because the α' form is transformed irreversibly [30]. The α form is usually considered as ordered and stable while the packing of chains in the α'-form is comparatively less ordered and more relaxed. Moreover, the unstable α' crystalline form induces lower thermal and mechanical stability [29]. As the T_m of α' is lower, it can be easily converted into the α form by increasing temperature [30].

The β structure of PLA has a melting temperature that is approximately 10°C lower than that of the α crystal, suggesting that it is thermally less stable. The β crystals are created by stretching the α structure at elevated temperature and high draw-ratio, for example in hot-drawing of melt. It comprises a frustrated structure with a trigonal cell that randomly contains three chains oriented in both up and down directions [31].

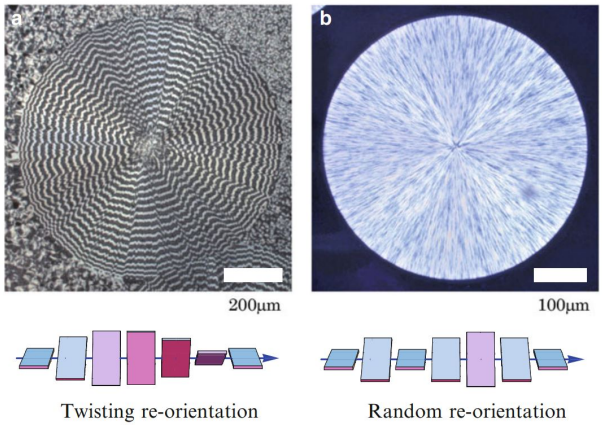

Figure 2.5: Ring-banded (*on the left*), and non-banded (*on the right*) spherulites seen with POM, taken from [25].

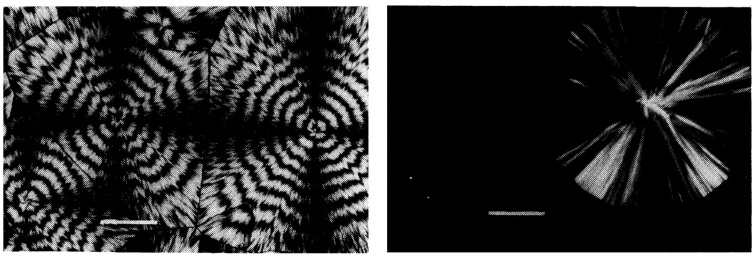

Figure 2.6: POM micrographs of banded-spherulites of PLA/PEG 50/50 (*on the left*), and non-banded spherulites of pure PLLA (*on the right*). Scale bar indicates 100 μm, taken from [32].

On the other hand, the γ form of PLA, which is obtained via epitaxial crystallization of PLA on hexamethylbenzene, consists of two chains oriented antiparallel in the crystal cell, and it is more ordered that the β form [31]. This crystal system is orthorhombic and is based on a three-fold helix conformation [33].

Apart from the homo-crystallization of pure PLLA and pure PDLA, these two enantiomeric chains can also co-crystallize to create a stereocomplex. Interestingly, the melting point of the stereocomplex is approximately 50°C higher than that of the PLA homo-crystal. Thus, stereocomplexation could provide a material with greater temperature resistance [31].

PLA presents a glass transition temperature (T_g) of about 60°C which is relatively low compared to other polyesters. Therefore, in order to enhance its thermal resistance, PLA has to be crystallized to a large extent [31].

Crystallization kinetics

When examining the overall crystallization kinetics of polymers, two distinct processes are typically considered: initial crystal nucleation and subsequent crystal growth [31]. Nucleation is the initiation from a solution, a liquid, or a vapour during which a few organized prenuclei are formed. Their structure is in line with the crystalline motif. Some of these prenuclei will dissipate while the radius of the others will grow until a critical size and these prenuclei will become stable nuclei [34]. Two forms of nucleation are distinguishable: homogeneous and heterogeneous nucleation. We talk about the first one when the critical nucleus emerges in the homogeneous bulk and about the second one when the nucleus is formed heterogeneously on a surface or on an impurity. Heterogeneous nucleation reduces the surface free energy and so the nucleation barrier of the emerging nucleus too. Consequently, this nucleation is often faster than the homogeneous one [35]. Molecular mobility and molecular interactions as well as thermodynamic driving force can influence nucleation. During the crystal growth process, the nuclei grow and lead to a crystalline solid [34].

The number of spherulitic nuclei and so the density of spherulites tends to decrease as the temperature rises, and this decrease occurs at a progressively faster rate at higher temperatures. At a given temperature, the number of nucleation sites is constant with time. However, the radius of spherulites grows with time. Spherulites grow at the same rate until they meet each others [30, 31]. In addition to temperature, the concentration of D-lactate is also a factor that affects the growth rate of PLA crystals. As the optical impurity increases, the maximum spherulite growth rate decreases significantly. Research conducted by Saeidlou *et al.* [31] has suggested that the optimal crystallization temperature (T_c), at which the crystal growth rate is highest, falls within the range 115-130°C. The maximum growth rate of PLA crystals is affected by the molar mass of the polymer. This

is because higher molar mass leads to more restricted chain mobility, resulting in a decrease in the growth rate. The flexible nature of the PLA polymer chain is attributed to the presence of an oxygen atom in the backbone. This oxygen atom allows for a nearly free rotation around the O-C bond, which leads to a more coiled chain. In terms of crystallization, this flexibility implies that the chain must overcome a higher entropy barrier in order to crystallize.

2.1.4 Limitations

The most important limitations of PLA are its lack of hydrophilicity as well as brittleness and low fracture toughness [18].

PLA hydrophobicity results in a low cell affinity and could induce an inflammatory response from the host [9].

PLA exhibits an elongation at break lower than 10%. For biomedical applications that require plastic deformation at a high stress level such as screws and fracture fixation plates, PLA has a too poor toughness.

Even though it is degradable, PLA presents a slow degradation rate and long reabsorption time. It means that the polymer degrades and is absorbed by the body at a slower rate, so that the polymer has a long *in vivo* lifetime, which can reach years [9]. A slow reabsorption time can increase the risk of long-term complications, such as chronic inflammation or foreign body reactions. In addition, slow-reabsorbing polymers may not be suitable for certain applications where rapid tissue regeneration is needed, such as in wound healing [36].

PLA also presents a slow crystallization rate. It can induce amorphous phases presenting low mechanical properties and thermal stability, which can limit its use as medical product [30].

In order to overcome these limitations, PLA can be modified. Blending of PLA with other biocompatible hydrophilic polymers allows to take advantage of PLA properties while minimizing its disadvantages [18].

2.1.5 Biomedical applications

PLA is an interesting polymer for biomedical applications. Indeed, it can be used in a wide spread of applications by simply modifying its physical-chemical structure. PLA is often blended with other polymers (or with non-polymeric components) to achieve the desired behavior [6]. PLA can be used for ligament attachment, soft-tissue implants, tissue engineering scaffolds, drug delivery devices, etc [37].

Tissue engineering

Transplantation of organs or tissues can be a treatment option for patients with damaged or diseased organs or tissues. However, there is a significant shortage of donors available. Tissue engineering offers an alternative approach to construct biological replacements that can help restore and maintain normal function in damaged and diseased tissues [38]. Tissue engineering involves many different research fields such as medicine, biology, materials science and engineering. Tissue engineering aims at designing a biomaterial scaffold as a transplantable construct on which cells are seeded and grow along with growth factors, as schematically shown in Figure 2.7. The goal is to enable regeneration of functional tissue in the host [39]. Scaffolds usually act as artificial supporting matrices, taking the shape of native tissues in order to mimic their characteristics [19]. The cells seeded on the scaffold can be either heterologous (such as bovine), allogeneic (same species, different individual), or autologous (from the patient itself) [38].

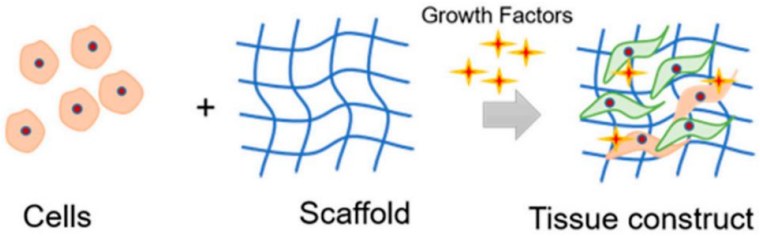

Figure 2.7: Basic tissue engineering principle, taken from [40].

To create a tissue-engineered construct, a scaffold must fulfill certain functions and therefore have certain properties. It should allow:

- Transportation of essential nutrients required for cell adhesion, proliferation and differentiation [41]. For this purpose, the scaffold must possess an open-pore network, meaning that the scaffold must be porous and the pores interconnected [42].
- Promotion of cell-biomaterial attachment, growth and migration [41]. A scaffold must therefore mimic the extracellular space it replaces for a proper cell function and development [43].
- Provision of mechanical support [41]. The mechanical properties of the scaffold such as its elastic modulus must be as close as possible to the properties of the tissue it replaces [44].
- Controlled degradation rate without any toxicity or risk of inflammation to the cells [41]. Hydrophilic materials degrade at a faster rate.

Thanks to its excellent thermal stability, processability, and biocompatibility, PLA has already been used for some applications in dentistry, musculoskeletal, and orthopedics sectors. Prominent applications of PLA include bone, neural, skin, cartilage, ligament, and vascular regeneration. For example, PLA-based filaments can be applied in musculoskeletal tissue engineering applications for substituting fibers and ligaments [19]. Three-dimensional (3D) PLA scaffolds were already made using electrospinning process and 3D-printing for bone tissue regeneration. Ritz *et al.* fabricated a scaffold of PLA coated or filled with collagen by 3D-printing and demonstrated the potential of 3D-printed PLA scaffolds for bone tissue regeneration. Indeed, the scaffolds presented rapid vascularization ability and robust osteoinduction bioactivity [6]. PLA was already studied by Lee *et al.* to be used for cardiovascular tissue engineering. They developed a 3D-printed PLA-based biodegradable polymeric stent for the prevention of thrombosis and restenosis. The stent showed good blood compatibility and anticoagulation [19].

2.2 PLA/PEG blends

Biomaterial scaffolds must meet certain properties. This is why, to select a polymer for blending with PLA to create a biomaterial, many criteria have to be taken into account such as compatibility, lack of toxicity, degradability, etc. The most common polymer used as plasticizer for PLA is PEG due to its partial miscibility with PLA [45]. Blending of PLA with PEG allows to modify its bulk microstructure and surface properties [46]. The addition of PEG to PLA allows for example to induce porosity and increase the hydrophilicity of the product. A great advantage of blending is that, by simply varying the component ratio of PLA and PEG, mechanical properties and degradation rates can be modified [13].

2.2.1 PEG properties

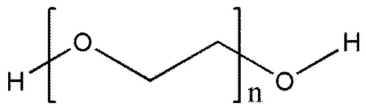

Figure 2.8: PEG structural formula, taken from [47].

Poly(ethylene glycol) (PEG) is a polyether approved by the FDA and is popular due to its tunable properties. PEG can be synthesized via anionic polymerization of ethylene glycol with a hydroxyl initiator. PEG presents a high structure flexibility, biocompatibility, amphiphilicity and a high hydration capacity [48]. It is crystalline, nontoxic and hydrophilic [13]. Depending on its molar mass, it can be liquid or solid at room temperature. Below 700 g/mol, PEG is liquid at room temperature. Between 1000 and 2000 g/mol, it is a soft solid and above 2000 g/mol, it is a hard crystalline solid [48, 49]. T_g and T_m of PEG can range from -98 to -17°C and from 51 to 68°C, respectively [48]. Its T_c is approximately 40°C [32]. PEG is highly hydrophilic, it is soluble in water and in other organic and inorganic solvents. When blended or co-polymerized with hydrophobic polymers, PEG decreases the contact angle significantly. PEG has a plasticizing effect on other polymers such as PLA, meaning that the presence of PEG increases the chain mobility of PLA. It increases the flexibility and reduces glass transition temperatures and melting point of PLA/PEG scaffolds [13, 48].

2.2.2 Crystallization

Degree of crystallinity

It was found that increasing the PEG content in PLA/PEG blends enhances the crystallization of PLA, with a faster crystallization rate. Indeed, the presence of PEG decreases the viscosity, allowing PEG chains to diffuse more easily outside the spherulites, and decreases PLA chain entanglements, allowing PLA chains to move in an easier way [50]. The spherulitic growth rate is then increased. However, the presence of PEG decreases the density of nucleation sites. Indeed, PEG cannot act as heterogeneous nucleation site for PLA. Therefore, the addition of PEG allows to increase the spherulitic growth rate but decreases the nucleation density [51]. Overall, PEG improves the crystallization of PLA. Improving PLA crystallization allows to increase its modulus of elasticity, barrier properties, and thermal stability [30]. Younes and Cohn showed that, ranging from 1500 up to 35 000 g/mol, increasing the chain length of PEG increases the degree of crystallinity of PLA [52]. Moreover, Sungsanit *et al.* proved that, by increasing PEG content from 0 up to 20%, the degree of crystallinity of PLA is enhanced from 27 to 44% [45].

Figure 2.9 represents the relative crystallinity of PLLA as a function of time at different crystallization temperatures T_c. It is shown that the crystallization rate is much faster when PLA is blended with 30% of PEG. Moreover, from the graph of PLA/PEG 70/30 blend, it can be seen that the optimal T_c for PLA to crystallize faster is 110°C.

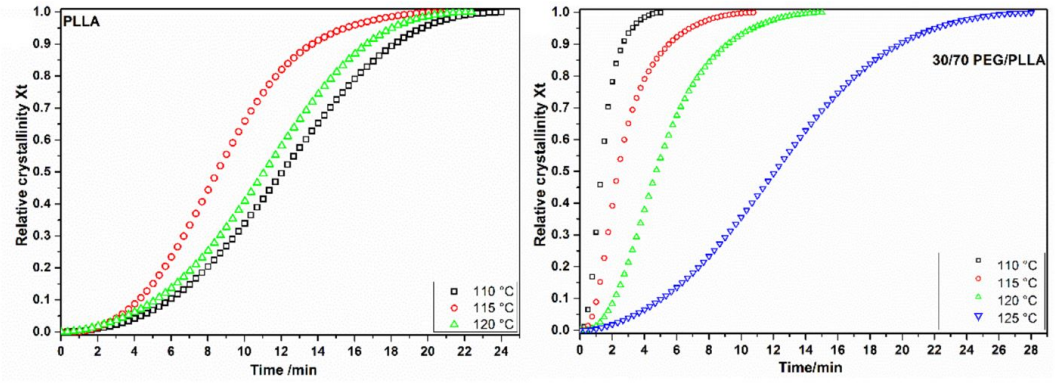

Figure 2.9: Relative crystallinity versus time at different crystallization temperatures for PLLA (*on the left*), and PLLA/PEG 70/30 blends (*on the right*), taken from [53].

Crystal structure

Melting and crystallization temperature of PLA depends on the weight fraction of PLA and PEG in the mixture. When blended with PEG, the T_m, T_g and T_c of PLA decreases to lower temperatures with increasing PEG concentration [32, 45, 46]. This decrease in temperature shows that there are interactions between both polymers chains: the presence of PEG significantly enhances the chain mobility [46].

In Figure 2.10 (a), it can be seen that during neat PLA crystallization, many small spherulites are formed. As shown in Figure 2.10 (b), when PLA and PEG are blended together, clear spherulites are also formed. The spherulites are fewer in number compared with neat PLA. It is explained by the fact that PEG decreases the density of nucleation sites. The size of the spherulites is a lot larger than the one of the spherulites formed during neat PLA crystallization. This phenomenon is due to the decreased nucleation density with the addition of PEG and to the fact that PEG facilitates the spherulitic growth of PLA. The crystallization of PLA is enhanced by the presence of the PEG plasticizer [13].

As the T_c of PEG is lower than the one of PLA, when cooling from the melt, PLA crystallizes first and PEG is ejected outside the growing crystals, segregating into interlamellar regions, and/or interfibrillar regions, and/or interspherulitic regions. It then crystallizes upon further ending if present in a sufficiently pure concentration (mainly in interfibrillar and interspherulitic regions). The spherulites are thus composed of PLA and PEG lamellar crystals as well as amorphous interlamellar regions. These ringed spherulites are a consequence of the strong effect of PEG molecules on the melting and crystallization of PLA [32].

Keith and Padden [54] developed a theory about spherulitic crystallization of polymers from the melt. This theory states that bundles of discrete fibers are formed during polymer crystallization from the melt and that their widths are determined by $\delta = D/G$, D being the coefficient of self-diffusion and G being the growth rate. Starting from this theory, when two molten polymers are blended together, there should exist a critical spherulitic growth rate of PLA above which PEG is trapped in the growing spherulites of PLA, and below which PEG has time to diffuse outside the spherulites of PLA [55]. This could be translated into the following formula: $D_{PEG}/G_{PLA,rad}$ with D_{PEG}, the diffusion coefficient of PEG in $\mathrm{m}^2\times\mathrm{s}^{-1}$, and $G_{PLA,rad}$, the radial growth rate of PLA spherulites in $\mathrm{m}\times\mathrm{s}^{-1}$. If the diffusion coefficient of PEG is higher than the radial growth rate of PLA spherulites, PEG has time to diffuse outside the growing spherulites of PLA and a part of the PEG aggregates in interspherulitic regions. On the contrary, if PLA spherulites grow at a faster rate, PEG is trapped in the growing PLA spherulites and mainly locate in interfibrillar regions.

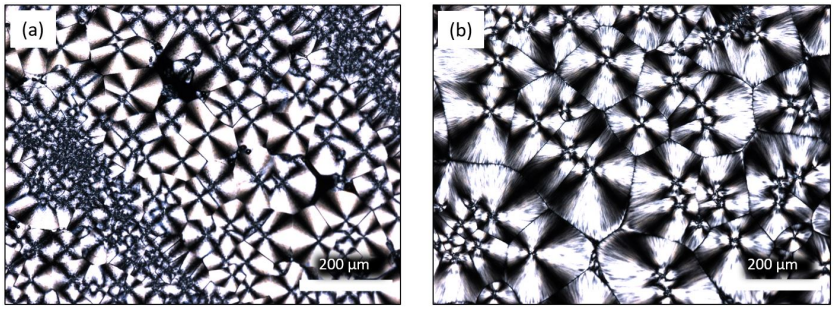

Figure 2.10: POM micrographs of (a) pure PLA, and (b) PLA/PEG 90/10 blend.

Phase separation

When PLA and PEG are melted together and are then crystallized from the melt, two different phase separations may occur: a liquid-liquid phase separation and a liquid-solid phase separation.

Liquid-liquid phase separation may occur when the two polymers are in the molten state. It is controlled by the interaction parameter of the blend. Flory-Huggins interaction parameter (χ_{12}) can be computed as follow [56, 57]:

$$\chi_{12} = \frac{V_1}{RT}(\delta_1 - \delta_2)^2 + B$$

with V_1, the molar volume of the first component (PLA), R the gas constant, T the temperature, δ_1 and δ_2 the solubility parameters of the blend components (PLA and PEG), and B the entropic component (between 0.3 and 0.4). Blends with $\chi < 0.5$ can be considered as miscible and no liquid-liquid phase separation is expected. The solubility parameter of a polymer changes slightly depending on its molar mass: the higher the molar mass, the smaller the solubility parameter. PLA with M_n 90 500 g/mol has a solubility parameter of 20.4 $\text{MPa}^{1/2}$ and PEG with M_n 1000 g/mol has a solubility parameter of 21.9 $\text{MPa}^{1/2}$ [56, 57].

Liquid-solid phase separation may occur when PLA crystallizes in an homogeneous liquid blend (crystallization from the melt). Segregation of PEG (liquid phase) occurs due to crystallization of PLA (solid phase), with different final localizations (interlamellar, interfibrillar, or interspherulitic). This separation process depends on the PEG concentration.

A study conducted by Younes and Cohn [52] showed that when PLA and PEG are blended together, both will be able to crystallize if their content is higher than 20%. The blend created will contain two phases that are partially segregated, crystalline and dispersed in an amorphous matrix. When one of the two polymers has a composition smaller than 20%, it will not be able to crystallize, only the polymer with the highest concentration will crystallize. The minor component and

the amorphous phase of the major one will create a non-crystalline matrix.

2.2.3 Degradation rate

PEG is hydrophilic and presents a faster degradation rate than PLA. When the PEG content in PLA/PEG blends is increasing, water contact angle values decrease, indicating that the surface wettability is enhanced; the blend will therefore degrade at a faster rate [14]. When the scaffold is immersed in biological fluid, if the surface is hydrophilic, the absorption of water is promoted and the degradation rate is increased. Hydrophilicity promotes the hydrolysis process by which polymers degrade [58].

Serra *et al.* [14] prepared PLA/PEG blends with different PEG contents, varying from 0 to 20%. They tested the degradation rate of the blends by immersing them for 8 weeks in simulated body fluid (SBF) at 37°C. They showed that, the higher the PEG content, the higher the weight loss along the weeks. This indicates that the PEG increases the degradation rate of the blend. It is important to keep in mind that PEG is soluble in water and that the SBF solution has a chemical composition similar to the one of blood plasma, made up in large part of water. A part of the weight loss of the blends may therefore be due to the extraction of PEG in SBF.

2.2.4 Mechanical properties

Adding PEG to PLA decreases its tensile strength and elastic modulus but increases its elongation at break, as observed in Figure 2.11. When 10% of PEG is present in the PLA/PEG blend, the impact resistance is increased by more than five times the one of neat PLA. As the plasticizer content and molar mass decrease, the PLA blended with PEG exhibits increased brittleness. This is accompanied by a rise in plasticizing efficiency with decreasing molar mass of PEG. Conversely, when the molar mass of PEG is held constant, the material becomes brittle at higher PEG content due to insufficient cohesion between the spherulites, probably due to interspherulitic PEG segregation [45].

2.2.5 Biomedical applications

Tissue engineering

PLA/PEG blends are already actively studied to create biomaterial scaffolds. Salehi *et al.* [18] created PLA/PEG scaffolds by fused deposition modeling (FDM) 3D-printing in order to study its use as biomaterial for bone tissue engineering. They proved that increasing PEG content allowed to enhance the osteogenic capacity of

the mesenchymal stem cells (MSCs) grafted on the scaffold as well as osteogenic differentiation of MSCs, showing a higher osteogenic potential of PLA/PEG scaffolds compared to pure PLA scaffolds. They proved that PLA/PEG scaffolds exhibit improved cellular behavior (such as cell proliferation and adhesion), biocompatibility and osteogenic potential than pure PLA scaffolds, but lower mechanical properties. They concluded that PLA/PEG scaffolds fabricated by FDM 3D-printing can be a good choice for bone tissue engineering applications due to the excellent printability and also appropriate physical-mechanical and biological properties.

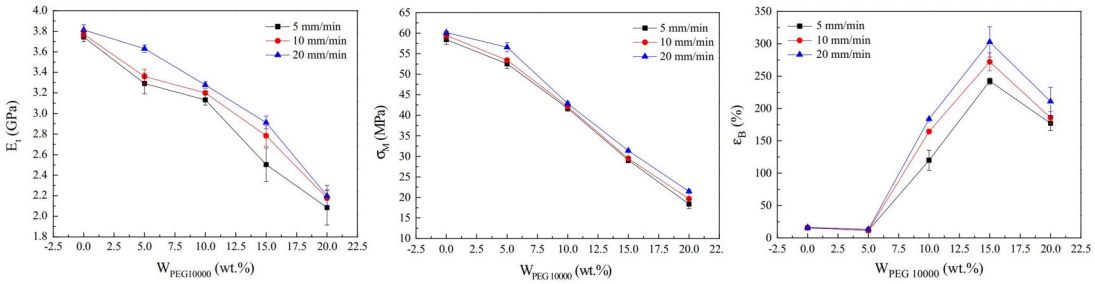

Figure 2.11: Young's modulus (*on the left*), tensile strength (*in the middle*), and elongation at break (*on the right*) of PLA/PEG blends as a function of PEG content at various tensile speeds, taken from [59].

Drug delivery

Nanoparticles of methoxy poly(ethylene glycol)/PLA (mPEG/PLA) blends were already designed for drug delivery. By varying the ratios of mPEG/PLA component in the blend, different properties such as drug loading, particle size and release profiles can be controlled [60].

Porous matrix films made of PLA/PEG were used for the delivery of the antibiotic gentamicin sulphate (GS) or metronidazole for wound dressing application. As already mentioned, PLA/PEG films exhibit higher porosity and pore size than pure PLA. This increases the rates of water vapor and oxygen transmission, degradation rate and total drug release [60].

2.3 The importance of porosity in scaffolds

2.3.1 Overview

In tissue engineering, cells are cultivated on a scaffold along with growth factors, in order to create synthetic human tissues [40]. A critical aspect of scaffolds is controlling porosity and microarchitecture to create engineered tissues with similar structure and function as native tissues. Scaffold porosity is particularly important for directing tissue formation and function, as it allows for homogeneous cell distribution and interconnection throughout the tissue. Moreover, increased porosity can facilitate the diffusion of nutrients and oxygen, which is especially important in the absence of a functional vascular system [61]. To present high porosity, a scaffold should have appropriate surface area and internal volume [13].

The mechanical properties of a scaffold are greatly influenced by its degree of porosity. An increasing porosity leads to a decreased stiffness. Pore architecture, particularly pore interconnectivity, also plays a significant role in cell behavior such as survival, proliferation, and migration. The ability of cells to grow into the pores is important for vascularization (formation of new blood vessels within the materials) and nutrient diffusion, and increasing pore size has been shown to enhance extracellular matrix (ECM) secretion. The size of the pores also affects the amount of contraction a graft undergoes after implantation, and there are optimal pore sizes for different types of tissue regeneration: 5 μm for neovascularization, 5–15 μm for fibroblast ingrowth, 20–125 μm for adult mammalian skin regeneration, 100–350 μm for bone regeneration, 40–100 μm for osteoid ingrowth, and 20 μm for hepatocyte ingrowth [61].

2.3.2 Porous scaffolds fabrication techniques

Scaffold fabrication techniques need to fulfill some requirements such as control of macrostructure and microstructure, and the maintenance of biocompatibility and mechanical properties. The pore architecture of scaffolds must be controlled because it is critical for cell survival and proliferation [62].

Various techniques already exist to create porous structures. For example, freeze-drying, and solvent casting/salt leaching have already been used to create porous scaffolds. However, these techniques present a few drawbacks such as lack of 3D structure and control on pore size and interconnectivity [62].

Electrospinning

Electrospinning is a technique that allows to fabricate porous scaffolds. This technique is based on the facrication of micro- and nanofibers. To create these fibers, a polymer solution or a melt is charged by a high voltage and passes through a syringe. The charged solution is directed toward a collector. On the way to this collector, the solvent evaporates and dry fibers are collected. An advantage of electrospinning is its flexibility. Indeed, a large range of materials can be used for electrospinning and the fiber morphology can be easily controlled. Parameters influencing fibers morphology are the molar mass and the concentration of the polymer, the properties of the solvent, and the electrical field applied during the electrospinning process. Another advantage is that it is possible to incorporate particles in the fibers. It can be useful in tissue engineering because it allows the controlled release of growth factors. Moreover, this technique allows to create scaffolds that mimic the extracellular matrix (ECM). As previously mentioned, a scaffold should present micro- and macroporosity. A studied technique used to achieve that is to combine nano- and microfibers in a scaffold. Unfortunately, there are problems finding a technique to mix the two different sets of fibers [63]. The main disadvantaged of electrospinning are the random orientation of the fibers, the non-uniformity of pore sizes and the high voltage requirements (1-30 kV) [64].

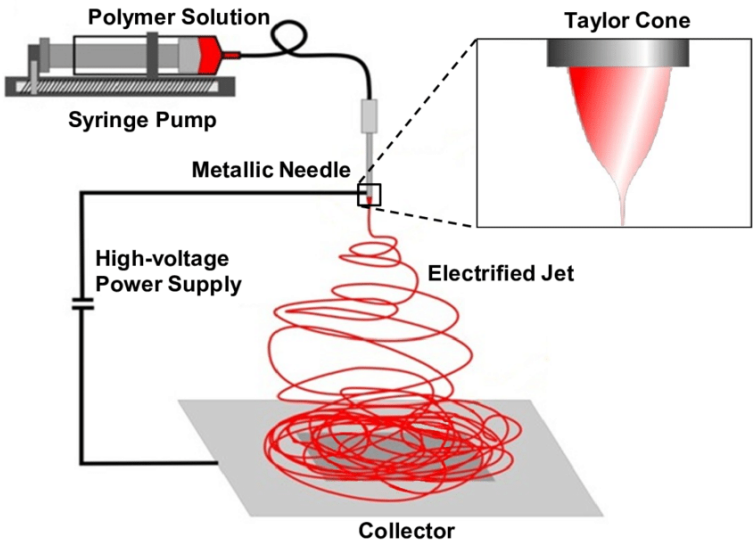

Figure 2.12: Electrospinning process - scheme, taken from [65].

Gas-based techniques

Conventional gas foaming In this technique, a chemical compound such as sodium bicarbonate is added into the polymer to create an inert gas such as N_2 or CO_2. This chemical compound is called a foaming agent. Gas bubbles, called internal phase, form and disperse throughout the polymer phase, called continuous phase. When the dispersed gas phase is removed from the polymer phase, pores remain at places where the bubbles were standing and a porous structure is created. A drawback of gas foaming is that the continuous phase which is liquid tends to move towards the bottom, while the internal phase which is gaseous tends to move upwards. The porosity is then non homogeneously distributed. In order to counteract this phenomenon, a surfactant can be added to the polymer solution to stabilize the foam [62].

Dense gas foaming It is a gas foaming technique that uses high pressure CO_2 as foaming agent. In order to induce highly interconnected porous structure, salt particles such as NaCl are commonly added to the polymer solution before gas foaming [62]. This process is called salt leaching. The salt particles are leached out by immersing the polymers in water and pores remain in the polymer structure [66]. However, leaching out a component might affect the structural morphology of the scaffold [63].

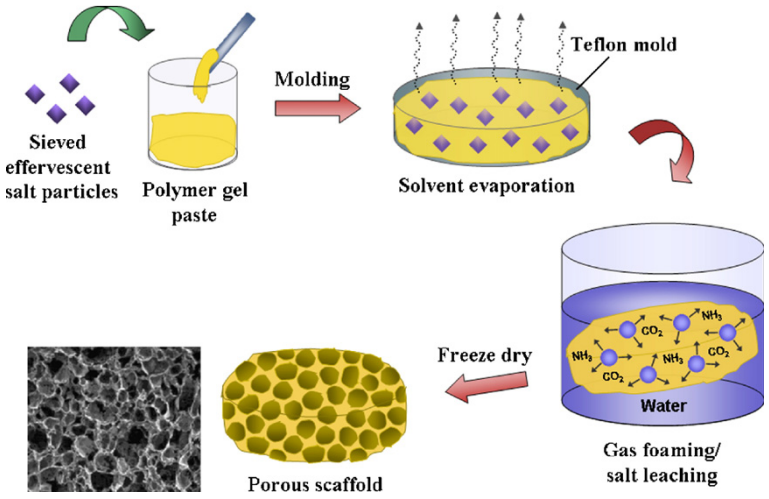

Figure 2.13: Gas foaming process - scheme, taken from [67].

3D-printing

Three-dimensional printing (3D-printing) is a technique that allows to fabricate defined scaffold structures with controlled pore size and interconnectivity. During 3D-printing, the scaffold is fabricated using a layer-by-layer process [64]. There are different techniques of 3D-printing such as selective laser sintering (SLS), stereolithography apparatus (SLA), inkjet 3D-printing, or fused deposition modeling (FDM) [68, 69].

Fused deposition modeling (FDM) is based on the melting and extrusion of a polymer filament. The polymer is first introduced in a heated metal cylinder ending in a nozzle. The polymer is melted in the cylinder. The filament is extruded from the nozzle and has a diameter similar to the one of the nozzle. In order to create the desired scaffold shape, the filament is deposited on a plate called the print bed at a certain distance, depending on the desired resolution. A first layer of polymer is deposited on the print bed by moving the nozzle and the print bed in perpendicular directions. The nozzle is then lowered by a fixed distance corresponding to the thickness of the first layer and a second layer is deposited on top of the first one, then a third layer and so on until the entire scaffold has been printed [68]. FDM is a technique that is easy to use, simple to operate, and that exhibits low cost in use and maintenance. It is mainly used with polymers presenting relatively low softening temperatures (melting temperature for semi-crystalline polymers; glass transition temperature for amorphous polymers) such as polylactic acid (PLA), acrylonitrile butadiene styrene (ABS), polycarbonate (PC), and polyamide (PA) [69].

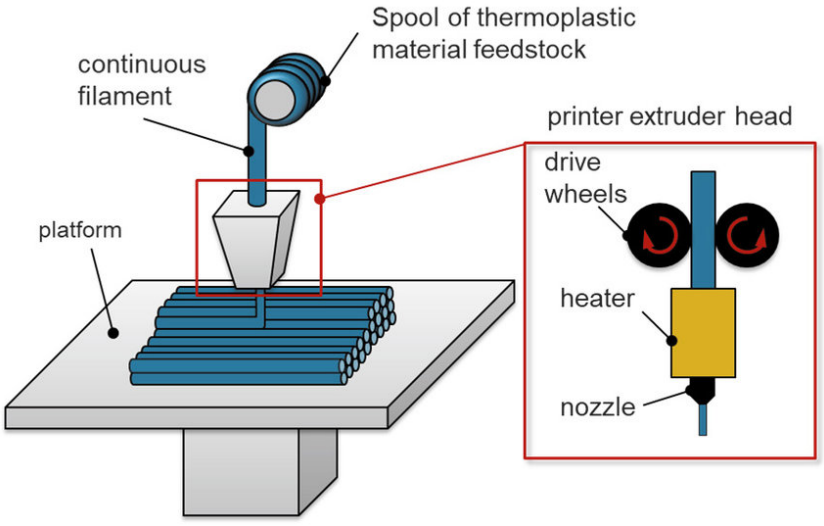

Figure 2.14: Fused deposition modeling process - scheme, taken from [70].

2.3.3 Porosity of PLA-based scaffolds

The porosity of a PLA scaffold can be computed as [10]:

$$Porosity(\%) = \left(1 - \frac{\rho_{scaffold}}{\rho_{PLA}}\right) \times 100$$

with $\rho_{scaffold}$, the density of the scaffold, and ρ_{PLA}, the density of PLA (1.24 g/cm^3). It expresses the ratio between the pore volume and the total volume of the scaffold [10, 11, 71].

Rodrigues *et al.* [72] studied porosity in PLA scaffolds. They created PLA porous scaffolds by laser cutting a PLA bar fabricated beforehand by 3D-printing. A uniform pore distribution and well-defined geometry is observed with SEM as shown in Figure 2.15.

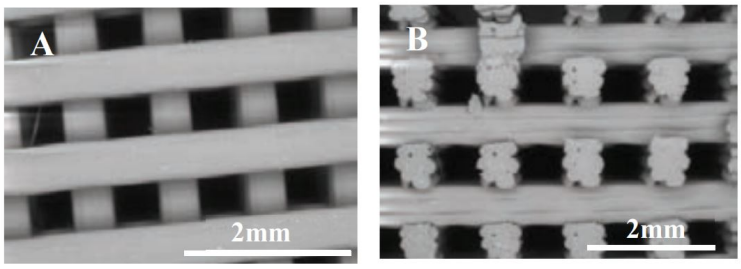

Figure 2.15: SEM images of laser cut PLA scaffold, (A) top view, and (B) middle cross-section, taken from [72].

Baptista and Guedes [73] created porous PLA scaffolds using 3D-printing. They fabricated scaffolds with three different porosity levels by changing the polymer filament offset distance (distance between the nozzle from which the filament is extruded and the printing bed). The diameter of the nozzle is the same for all printed scaffolds. By increasing the filament offset distance, the scaffold porosity as well as the pore size are increased. Scaffolds exhibiting a porosity of 30, 50, and 70% with a pore size of 171, 400, and 933 μm, respectively were created. During the 3D-printing process, the layers were stacked in two different configurations: orthogonal, as shown in Figure 2.16 (a-c), and isometric, as shown in Figure 2.16 (d-f). The width of the polymer filament is influenced by the offset distance, as well as by the printing temperature, speed and extrusion rate. Indeed, decreasing the offset distance decreases the filament stretching. A reduced printing temperature or a reduced printing speed leads to a reduced polymer flow through the nozzle and so a reduced filament stretching as well, resulting in a higher filament width.

When the porosity is increased, the pore size is also increased, along with the filament offset distance. Pore size is higher in orthogonal (100-300 μm) than in

isometric (10-60 μm) configuration. All scaffolds exhibit an interconnected porous structure with pore size lying from 10 to 300 μm, depending on the configuration and the printing parameters [73].

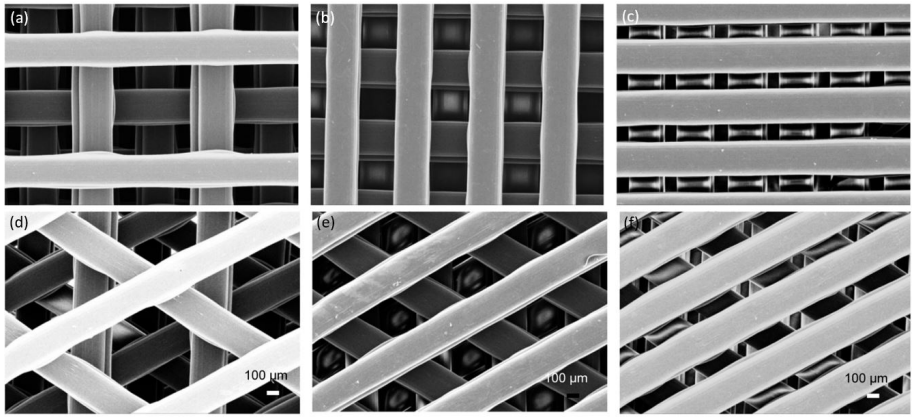

Figure 2.16: SEM images of 3D-printed PLA scaffold (top view). Orthogonal configuration with (a) 70%, (b) 50%, and (c) 30% porosity. Isometric configuration with (d) 70%, (e) 50%, and (f) 30% porosity. Taken from [73].

2.3.4 Porosity of PLA/PEG scaffolds

Chen *et al.* [13] studied the behavior of different PLA-based scaffolds fabricated by supercritical carbon dioxide (SC-CO_2) foaming and particle leaching. They blended PLA with PEG or NaCl, or both and leached out these compounds via deionized water in order to create an interconnected porosity. NaCl was used to create large pores while PEG was expected to create smaller pores. We will focus on the PLA/PEG blend. The concentration of PEG introduced in the blend was 10%. After being immersed in deionized water, the PEG content decreased to 5% in the total blend. The removed PEG induced porosity in the scaffold and the remaining PEG is not a problem as PEG is nontoxic, FDA approved, and hydrophilic. As can be observed in Figure 2.17, the viscosity of PLA/PEG blend is significantly lower than the one of pure PLA. Both pure PLA and PLA/PEG blend exhibit a Newtonian plateau at lower frequencies and exhibit a shear thinning behavior at higher frequencies. The complex viscosity of neat PLA is approximately 800 Pa×s while the one of PLA/PEG is about 200 Pa×s. It can be explained by the plasticization effect of PEG which increases chain mobility of PLA, increasing its flow and decreasing its viscosity. During the foaming process, this decreased viscosity could induce the rupture of pore wall during pore expansion which would create an open-porous structure.

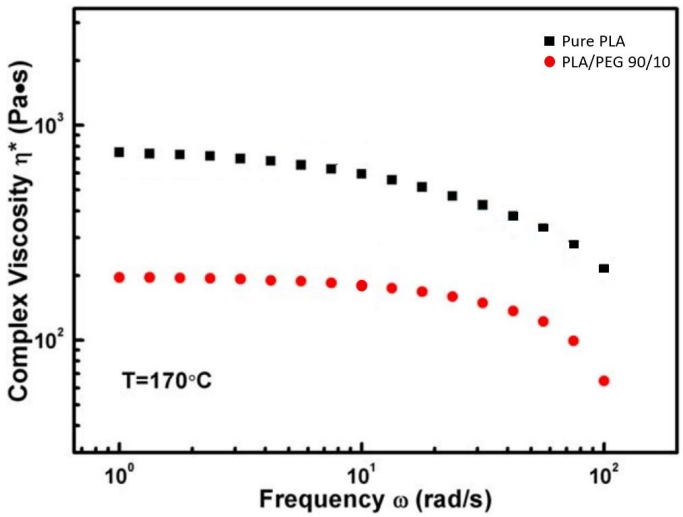

Figure 2.17: Complex viscosity ($\eta*$) as a function of frequency for pure PLA, and PLA/PEG 90/10 blend at the temperature of 170°C, adapted from [13].

As expected, it can be observed in Figure 2.18 that due to the plasticizing effect of PEG and moreover to the extraction of PEG, PLA/PEG 90/10 scaffold exhibits an open-pore structure with relatively thin pore walls while pure PLA scaffold has a closed-pore structure, induced by gas foaming, and thicker pore walls. The lower viscoelasticity of PLA/PEG blend leads to weaker pore walls. During pore expansion, the walls undergo rupture resulting in an open-pore and interconnected structure. In addition, when the PEG is extracted, pores remain at the locations previously occupied by the PEG [13].

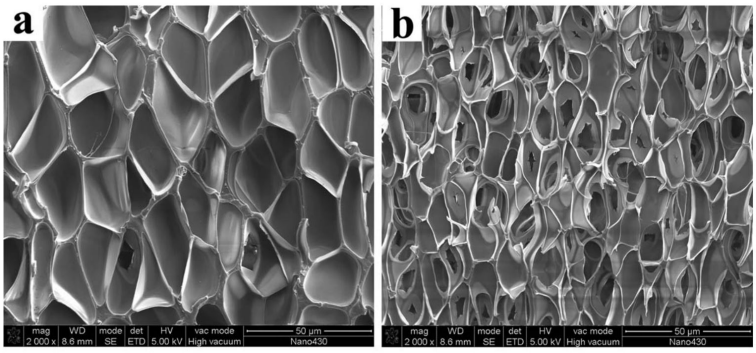

Figure 2.18: SEM micrographs of (a) pure PLA scaffold fabricated by SC-CO_2 foaming, and (b) PLA/PEG 90/10 scaffold fabricated by SC-CO_2 foaming, after PEG extraction. Taken from [13].

A study conducted by Yin *et al.* [74] confirm these conclusions. They also created scaffolds based on PLA, PEG, and NaCl particles in which PEG and NaCl particles are extracted using distilled water in order to induce porosity in the scaffolds. The scaffolds were fabricated by solid state extrusion and porogen leaching. In the melting extrusion of polymer/particles blend, a tradeoff between flowability and porosity must be achieved. They highlight that the presence of PEG decreases the viscosity and increases the flowability, leading to a favorable extrusion. More importantly, the extraction of PEG leads to a higher pore interconnectivity. Prior studies about PLA/PEG/NaCl blends showed that NaCl particles are often trapped within the matrix. As a consequence, the scaffolds exhibit unsatisfactory connectivity because the water cannot reach some NaCl particles when the scaffold is immersed in distilled water for extraction. The extraction of PEG creates interconnected channels that allow the removal of NaCl, leading to an increased porous structure. After the extraction of PEG and NaCl, they observed a highly interconnected porous architecture in three dimensions. In addition, the extraction of PEG induces a rough pore wall surface, which promotes cell attachment and proliferation.

Serra *et al.* [14] studied PLA/PEG scaffolds with 5, 10, and 20% of PEG, made by 3D-printing. They observed that when the PEG content is increased, pore size is decreased and the struts diameter becomes thicker. The porosity percentage of the 3D-printed scaffolds decreases from approximately 91% to 87% by increasing PEG composition from 5 to 20%. As can be observed in Figure 2.19, pure PLA scaffold exhibits rather squared pores and adopts a more rounded shape with the addition of PEG. The alterations in the size and geometry of struts and pores are linked to the significant reduction in viscosity observed in the polymer blends caused by the inclusion of PEG. The decreased viscosity resulted in a quicker and smoother flow of the polymer out of the printing tip, leading to struts that were less well-defined and less uniform in shape.

From these different studies, we can conclude that porosity and pore size of the scaffolds are influenced by the scaffold manufacturing technique. The presence of PEG in PLA/PEG blend decreases the viscosity compared to pure PLA. For manufacturing techniques such as foaming and leaching, it allows to increase the porosity [13, 15]. However, for 3D-printing, the fact that the polymer coming out of the printing tip is less viscous with the addition of PEG makes it more difficult to print well-defined struts and the porosity is slightly decreased [14].

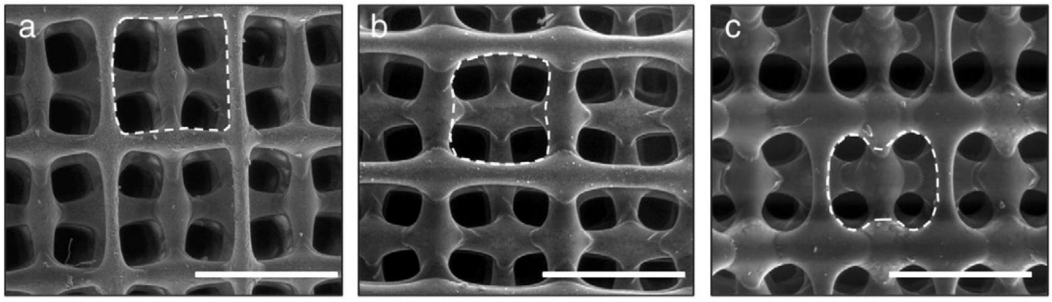

Figure 2.19: SEM micrographs of an axial view of (a) PLA/PEG 95/5, (b) PLA/PEG 90/10, and (c) PLA/PEG 80/20. Scale bar indicates 500 μm, taken from [14].

Cell viability

To be used as scaffold, as already mentionned, PLA requires certain properties such as good cytocompatibility, high porosity and high surface area with interconnected pore structure, in order to improve cell adhesion, proliferation and differentiation, and transport of nutrients to cells. To increase the open-cell structure in the PLA scaffolds, and so increase the porosity, PLA can be blended with another polymer such as PEG. A study conducted by Ren *et al.* [75], where they prepared PLA/PEG 60/40 scaffolds by the SC-CO_2 foaming technique, showed that the degree of opening cells of PLA/PEG blend was greatly higher than the one of pure PLA. It is important to highlight that open-cell content of polymeric scaffolds could provide an ample space for cell growth and activity. The open-cell content of pure PLA was approximately 35% while the one of PLA/PEG blend was higher than 80%. After proving that PLA/PEG blends were highly hydrophilic and open-porous, Ren *et al.* cultured NIH/3T3 cells (fibroblast cells) on the PLA and PLA/PEG scaffolds to test cell viability and proliferation. Before cell seeding, the blends were sterilized by immersion in 75% ethanol solution for 12h and then washed with phosphate buffered saline (PBS). As PEG is soluble in ethanol, PEG was inevitably extracted during the sterilization process. It can be observed in Figure 2.20 that over the days, the number of cells grows for both scaffolds, indicating that PLA and PEG are non-toxic for NIH/3T3 cells. However, we observe that there are many more cells on the PLA/PEG scaffold compared to the one made of pure PLA at the same incubation time. These observations demonstrate that the highly interconnected pore structure of PLA/PEG scaffold is favorable for cell attachment, growth and proliferation.

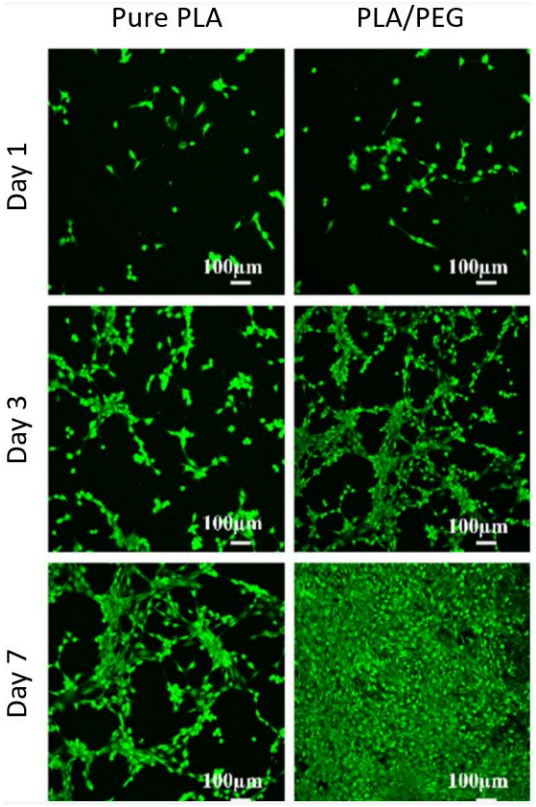

Figure 2.20: Cell fluorescence staining assay to evaluate the viability of NIH/3T3 cells cultured with PLA, and PLA/PEG 60/40 scaffolds (after PEG extraction), taken from [75].

Chapter 3

Objectives and Strategy

3.1 Objectives

In tissue engineering, an important parameter for the scaffold to be efficient is its porosity. However, by adding porosity to the scaffold, the mechanical properties will be lowered. A scaffold should therefore present a tradeoff between porosity which provides cell and nutrient diffusion through the scaffold, and mechanical properties which provide cell support and maintenance of the scaffold once implanted [76].

To fulfill its functions, a biomaterial scaffold needs to contain both micro- and macroporosity. Microporosity allows the diffusion of nutrients and oxygen, and macroporosity additionally allows the diffusion of cells in the material.

The subject of this study is the development of a 3D-printable porous biodegradable polymer material for biological applications. For this purpose, we will create PLA/PEG blends in the first place, induce phase separation between PLA and PEG, and then extract PEG to create pores at the areas where PEG was located before extraction. 3D-printing can induce macroporosity and PEG extraction can induce microporosity.

PLA is a promising polymer for biomedical applications and is increasingly studied. It is biocompatible and presents suitable mechanical properties for tissue engineering [36]. It has already been used in some biomedical applications, as discussed in Chapter 2. However, PLA is not porous and, as previously mentioned, a biomaterial must be porous to fulfill its functions. Moreover, PLA is hydrophobic and has a slow degradation rate and long reabsorption time, meaning that the polymer degrades and is absorbed by the body at a slower rate [4, 36]. The degradation rate of a scaffold should be proportional to the rate at which the body makes new tissue. The slow degradation rate of PLA may be a problem for some applications needing a faster degradation such as drug delivery devices. PLA

usually requires years to degrade completely but it can lose its tensile strength in only a few weeks [36].

In this study, the aim is to create a porous biomaterial and to control its porosity. When inducing porosity by extracting PEG from PLA/PEG blends, porosity is influenced by two main parameters: the molar mass of PEG and the composition of the blend. PLA will therefore be blended with PEG of different molar masses and concentrations.

PEG is hydrophilic and biocompatible and has a plasticizing effect on PLA. The incorporation of PEG in PLA facilitates the 3D-printing process thanks to its plasticizing effect and provides structural and physico-chemical changes to the printed scaffold [14]. Adding PEG to PLA proved to increase surface roughness and wettability, increasing the scaffold degradation rate [14]. Moreover, by extracting the PEG, the contact surface of the scaffold with water is increased when implanted in the body and the degradation rate is increased as well. It also induces roughness in the material, which allows cells to adhere more easily.

A previous study made in the lab examined PLA/PEG blends at different concentrations (90/10, 70/30 and 50/50) and with different PEG molar masses (3350 and 10 000 g/mol). In this study, the porosity was observed on the surface of the material. It was found that both PEG concentration and PEG molar mass influence porosity and pore size [50]. In this current study, we will analyse the porosity of different PLA/PEG blends inside the material rather than on the surface. Indeed, the properties of a material can vary between the interior of the material and its surface, and the inside of the material is more representative than the surface. We will focus mainly on PLA/PEG 70/30 and 50/50 blends. Indeed, blends of these concentrations present a higher porosity and are therefore more promising for biomedical applications.

PLA/PEG blends were already studied with rather small molar masses of PEG. While studying PLA/PEG blends, we will use three different molar masses of PEG in order to induce different porosity and pore size, and to study the effect of these PEG molar masses on PLA/PEG blends. PEG 3350 g/mol will be used so that a small molar mass remains to compare small and high molar mass. PEG 100 000 g/mol will also be used. Since the PLA used in this study also has a molar mass of 100 000 g/mol, this will allow us to analyse the effect of the molar mass when the latter is the same for the two polymers of the blend. Finally, PEG 1 000 000 g/mol will be used to study the effect of higher molar masses.

3.2 Strategy

Several samples of PLA/PEG blends will be studied. To prepare the samples, the first step is to make PLA/PEG films of the desired concentrations. To do so, PLA and PEG are first dissolved in chloroform ($CHCl_3$) and the chloroform is evaporated to obtain PLA/PEG films. Then, PLA/PEG films are crystallized. Thanks to hot presses, the films are heated to 200°C in order to melt the polymers; they then undergo a plateau at 170°C to rehomogenize without crystallizing, and finally the crystallization takes place at 110°C for 4 hours. The PEG is extracted via distilled water (PLA does not dissolve in water) and a porous sample is obtained. With the aim of observing the morphology inside the samples with a polarized optical microscope, sections of approximately 700 nm thickness are made with a microtome at room temperature and are deposited on a glass slide. In order to observe the porosity inside the samples using scanning electron microscopy, the samples are cut with a blade, stuck on aluminum foil with double-sided conductive tape, and the cut slice of the sample is observed.

Different compositions and molar masses of PEG will be studied:

- **Blends composition:** PLA/PEG blends with 30 and 50 wt% of PEG will be studied.
- **PEG molar mass:** MM-3350 g/mol (PEG 3K), MM-100 000 g/mol (PEG 100K) and MM-1 000 000 g/mol (PEG 1M) will be studied.

In order to analyze the effect of PEG content and the effect of PEG molar mass on the morphology of the samples, polarized optical microscopy (POM) is used. To study the effect of PEG content and PEG molar mass on the porosity of the samples, the size of the pores, and the spatial distribution of the porosity in the material, scanning electron microscopy (SEM) is used. Finally, the effect of PEG molar mass on the morphology and the porosity of the samples is studied at different depths inside the material and in 3 dimensions using confocal laser scanning microscopy (CLSM). The overall strategy is shown in Figure 3.1.

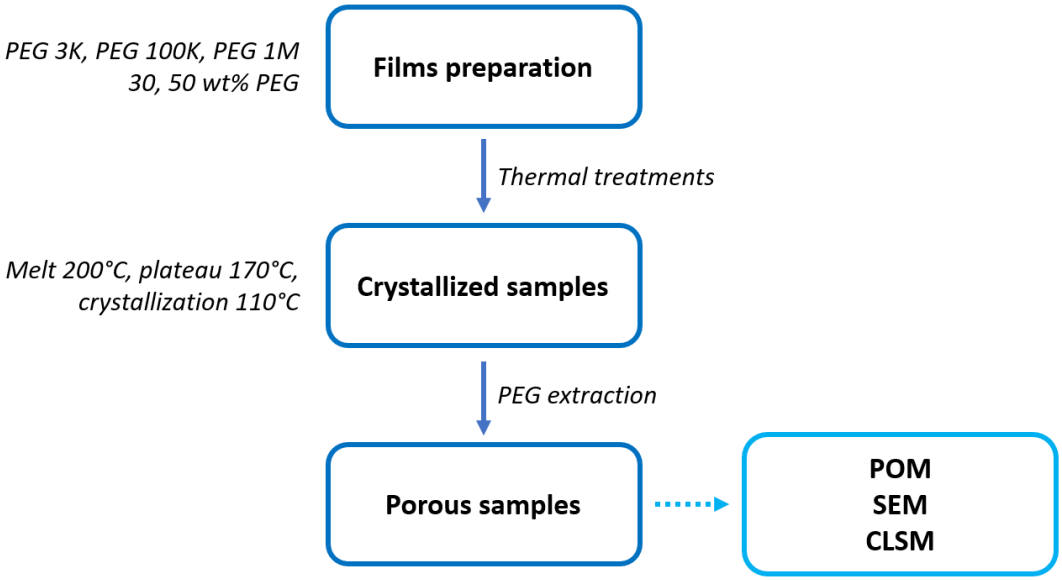

Figure 3.1: Overall strategy.

Chapter 4

Materials and methods

4.1 Materials

Poly(lactic acid) IngeoTM PLA HP2500 pellets were purchased from NatureWorks. Poly(ethylene glycol) PEG powder with M_n 3350 g/mol (PEG 3K), M_n 100 000 g/mol (PEG 100K), and M_n 1 000 000 g/mol (PEG 1M) were obtained from Sigma-Aldrich. Chloroform ($CHCl_3$) was also purchased from Sigma-Aldrich and used as acquired. Rhodamine 6G was purchased from Sigma-Aldrich.

4.2 Films preparation

Different PLA/PEG blend films were prepared. Two different concentrations by weight were used: 50% and 30% of PEG; and three different molar masses of PEG were used: 3350, 100 000, and 1 000 000 g/mol. In total, two films of six different blends were prepared: PLA/PEG 3K, 100K, and 1M 70/30, and PLA/PEG 3K, 100K, and 1M 50/50. Because both PLA and PEG are soluble in chloroform, it was used as solvent.

PLA pellets and PEG powder were first vacuum dried at 50°C for one night. The polymers were then placed in a beaker to have a total of 400 mg of polymers. For PLA/PEG 70/30, 280 mg of PLA and 120 mg of PEG was used, and for PLA/PEG 50/50, 200 mg of each polymer was used. A magnetic bar was added in the beaker. In order to have a concentration of 40 mg/mL, 10 mL of chloroform was added to the polymers. The beaker was covered with aluminium foil in order to avoid chloroform evaporation and placed on a stirring plate. The solution was stirred at 380 revolutions per minute (rpm) until full dissolution of the polymers. The solution was then transferred into a 90 mm diameter glass Petri dish in order to obtain a round flat film. A beaker was placed above the glass Petri dish so that the chloroform would evaporate slowly. After one night, a thin film was obtained.

The film was then peeled intact from the casting surface and stored in a plastic Petri dish under ambient conditions before further analysis. The whole process takes place at room temperature.

4.3 Isothermal crystallization

The isothermal crystallization of the films was performed by a thermal process. The thermal treatment consists of three steps. First, the polymers are melted at 200°C, then they go through a plateau at 170°C, finally they are set at 110°C for crystallization.

Two thin metallic sheets were needed and were covered with aluminium foil in order to work in a clean environment. A Kapton sheet was placed on a first metallic sheet in order for the sample to be easily removed after the treatment. A mold made from thicker aluminium was placed on the Kapton sheet. A film of PLA/PEG previously prepared was cut into small pieces that were then put in several layers inside the mold. A second Kapton sheet was placed on the mold and the second metallic sheet was placed on top of the first one, recovering the prepared mold. A scheme of the process is shown in Figure 4.1.

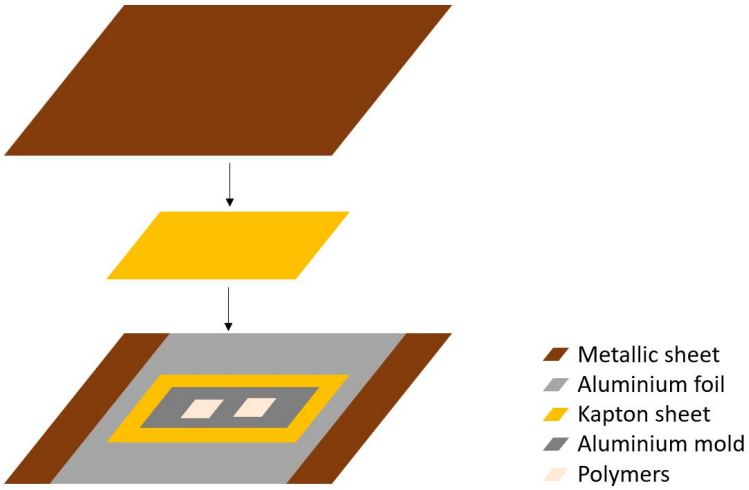

Figure 4.1: Scheme of the preparation for isothermal crystallization process.

The metallic sheets were then placed in a hot press machine at 200°C for 5 minutes so that the polymers would melt. The air bubbles eventually formed between the film layers were removed by increasing the pressure applied by the hot press machine on the metallic sheets to 5 MPa and bringing it back to 0 MPa. The process was repeated 10 times. The temperature was then decreased to 170°C

for 10 minutes (it took approximately 20 minutes for the temperature to decrease from 200 to 170°C). Finally, the metallic sheets were rapidly transferred to another hot press machine at 110°C and held at this temperature for 4 hours so that the polymer blend would crystallize.

The metallic sheets were removed from the hot press machine and were cooled down for 15 minutes at room temperature. The metallic sheet on the top was then removed as well as the Kapton sheet and the crystallized films were peeled off and stored in small rectangular plastic boxes under ambient conditions before further treatment.

4.4 Extraction method

In order to extract PEG from the prepared films, distilled water was used. Beakers were filled with distilled water and one sample of each blend was immersed in a beaker. The beakers were placed on a stirring plate at 80 rpm at room temperature. The films were immersed for 1h, 1h again and 24h. The water was changed each time to avoid PEG saturation in water. Samples were then dried for one night at room temperature.

4.5 Sections of the samples

Sections of the samples were realised using a Cryo-ultra microtome Reichert. The films were first placed in resin before cutting slices. The microtome sections were taken at room temperature, with a thickness of around 700nm. The sections were placed on glass slides.

4.6 Characterization techniques

4.6.1 Polarized-light optical microscopy

The morphology of the materials was examined between crossed polarizers using an Olympus AX70/Provis equipped with a charge coupled device (CCD) camera. The samples and their sections were put on a glass slide before observation at room temperature. Objectives of x10 and x50 were used. Images of the samples were recorded using the CCD camera. The CDD camera has two different modes: one for grayscale images and another for yellow/brown images. The colors of the POM images have no meaning; they are simply there to facilitate observation.

4.6.2 Scanning electron microscopy

Scanning electron microscopy (SEM) uses a focused accelerated electron beam as a source and allows to obtain images of high magnification with high resolution. To be analyzed with SEM, samples have to be electrically conductive to avoid overcharging on the surface. As polymers are not conductive, they are first sputter-coated with a thin layer of metal such as gold or chrome. The sample is then fixed to the sample holder with carbon tape and introduced in the sample-holding chamber or specimen chamber [77].

The porosity of the materials was examined using a JEOL 7600F (Japan). In order to observe inside the material, the samples were first cut using a blade so that we could observe the slice of the sample. They were then sputter-coated with a 12 nm-thin layer of gold with a sputter coater (Ted Pella, Cressington208HR High Vacuum Turbo Sputter Coater) before SEM observation, to be electrically conductive. The samples were stuck on aluminum foil with double-sided tape and then introduced into the sputtering device, with the slice previously cut with the blade upwards, facing the gold cathode. For SEM imaging, the samples were deposited on an adapted sample holder using double-sided conductive tape. All samples were observed in Secondary Electron Imaging (SEI) mode, with either Low Magnification (LM) or higher magnification (SEM) with an acceleration voltage of 5 kV at a working distance of 8 mm.

4.6.3 Confocal laser scanning microscopy

To image the samples with confocal laser scanning microscopy (CLSM), we first need to make them fluorescent. To do so, we used rhodamine as a dye. One drop of rhodamine was mixed with 15 mL of water and the mixture was used to color the samples. The sample is first immersed in the mixture for 30 minutes. The sample is then placed on a glass slide, a drop of the mixture rhodamine/water is deposited on the sample and it is covered with a cover slip. It is stored protected from light with aluminum foil at room temperature before further analysis.

Chapter 5

Results and discussion

To assess the influence of PEG molar mass and concentration on scaffold porosity, three different PEG molar masses (PEG 3K, 100K, and 1M) as well as two different PEG contents in the blend (30 and 50 wt%) were tested. All films were produced in the same way. However, PLA/PEG 3K 50/50 was not further analyzed because the films were of too poor quality after crystallization. Indeed, when the crystallized films were removed from the aluminium mold in which they underwent isothermal crystallization, they broke up into lots of little pieces because they were too fragile.

All the images presented in the following sections, whether they were taken with POM, SEM, or CLSM, were taken and analyzed after the extraction of PEG from the samples. As a reminder, the sections observed with POM were made with a microtome and deposited on a glass slide. To observe inside the samples with SEM, the samples were cut with a blade and the cut slice was observed. CLSM allows to observe inside the sample without cutting it, the entire sample is simply deposited on a glass slide and covered with a cover slip.

5.1 PEG localization after blend crystallization

As explained in Chapter 2, when PLA and PEG are blended together in the melt, they can be miscible or semi-miscible. When crystallization occurs from the melt at 110°C, PLA crystallizes first while PEG stays in the liquid state and liquid-solid phase separation occurs. During PLA crystallization, PEG diffusion takes place: the PEG diffuses outwards from the spherulites but a part of the PEG remains trapped inside the PLA spherulites. PEG can reside at three different locations within the crystallized blend: between PLA spherulites, between the stacks of PLA lamellae (called fibrils), and between PLA lamellae. The regions where PEG will be located after crystallization depends on its diffusion coefficient relative to the growth rate of PLA spherulites, according to the formula: $D_{PEG}/G_{PLA,rad}$. If the diffusion coefficient of PEG is higher than the radial growth rate of PLA spherulites, PEG will have time to diffuse out of the spherulites and a large part of the PEG will be located between the spherulites, in interspherulitic regions. On the contrary, if the radial growth rate of PLA spherulites is higher, PEG will be retained inside the PLA spherulites and will locate mainly between the fibrils and between the lamellae. If the melt is further cooled, PEG can crystallize if present in large regions such as interspherulitic or interfibrillar regions.

Interspherulitic regions

During PLA crystallization, PEG diffuses outside the spherulites and can accumulate in interspherulitic regions, as schematically depicted in Figure 5.1. At this point, the PEG rich regions will take a channel shape because they are wedged between two spherulites. Since a sufficient amount of PEG is present, the PEG will be able to crystallize during cooling. When the PEG is extracted, holes remain between the spherulites. In Figure 5.1, PEG located in interfibrillar regions is also represented as is explained in more detail below.

Interfibrillar regions

During PLA crystallization and PEG diffusion, some of the PEG can get stuck between the fibrils of the PLA crystals, as schematically shown in Figure 5.2. The PEG regions rather form pockets at this location. Here again, PEG can crystallize and holes will remain after PEG extraction.

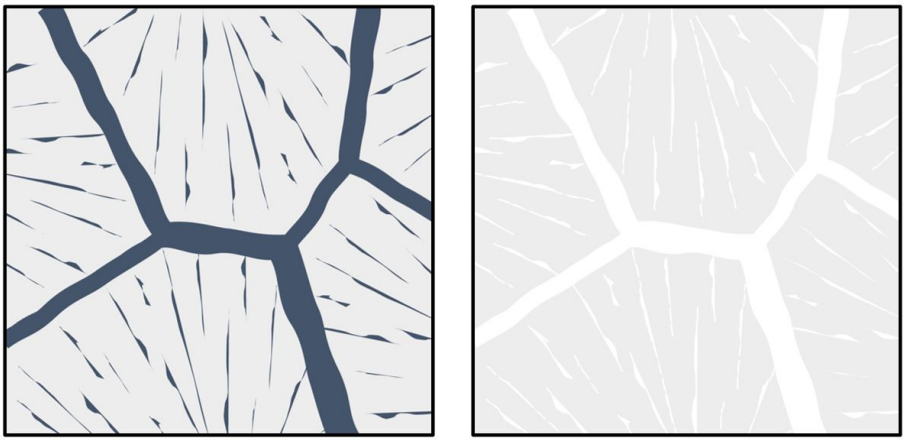

Figure 5.1: Schematic representation of the PLA/PEG blends before (*on the left*), and after (*on the right*) extraction - Interspherulitic regions. PLA is represented in grey and PEG in blue. Porosity is represented in white.

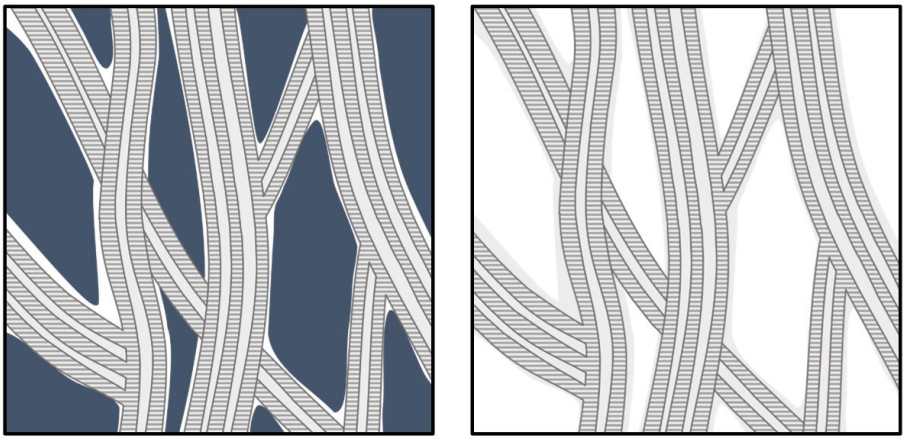

Figure 5.2: Schematic representation of the PLA/PEG blends before (*on the left*), and after (*on the right*) extraction - Interfibrillar regions. PLA is represented in grey and PEG in blue. Porosity is represented in white.

Interlamellar regions

Finally, PEG chains can be trapped between the lamellae of PLA crystals, as schematically shown in Figure 5.3. At this point, since the PEG chains are mixed with the amorphous phase of PLA and do not form PEG-rich regions, the PEG cannot crystallize easily and will stay in the amorphous state. When the blend is immersed in distilled water to extract the PEG, some chains will dissolve and will be extracted and others will stay intertwinned with PLA chains. Typically, as was

found in another study, about 5% of PEG remains in the total concentration of the sample after extraction. As previously said, PEG is nontoxic for the human body and degradable. It is then not a problem if some PEG remains in the scaffold material.

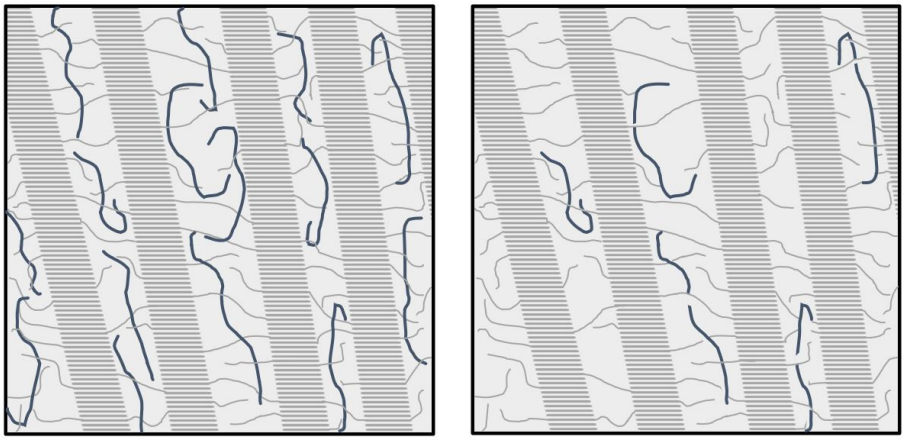

Figure 5.3: Schematic representation of the PLA/PEG blends before (*on the left*), and after (*on the right*) extraction - Interlamellar regions. PLA is represented in grey and PEG in blue. Porosity is represented in white.

The porosity of the blends will be studied on SEM micrographs. We will distinguish interspherulitic porosity and interfibrillar porosity. Indeed, the channels and the pockets of PEG present in interspherulitic and interfibrillar regions create porosity when extracted. However, when the interlamellar PEG is extracted, as only a few chains are present in the amorphous phase of PLA, no porosity will be generated.

5.2 Effect of PEG concentration

5.2.1 Morphology of the blends

Blends made with PEG 100K

POM micrographs of PLA/PEG blends made with 50 and 30% of PEG 100K are depicted in Figure 5.4. Images (a) and (b) were taken on the surface of the samples and images (c) and (d) were taken on the section of the samples. In Figure 5.4 (a) and (b), banded-spherulites clearly appear all over the surface and some black aggregates having a channel shape are observed in interspherulitic regions, some of these black aggregates are pointed with a white arrow. In Figure 5.4 (c), on the section of the PLA/PEG 100K 50/50 blend, elongated cracks appear inside the spherulites, some of these cracks are pointed with a white arrow. They are probably interfibrillar pores, indicating that some PEG was located between the fibrils before extraction.

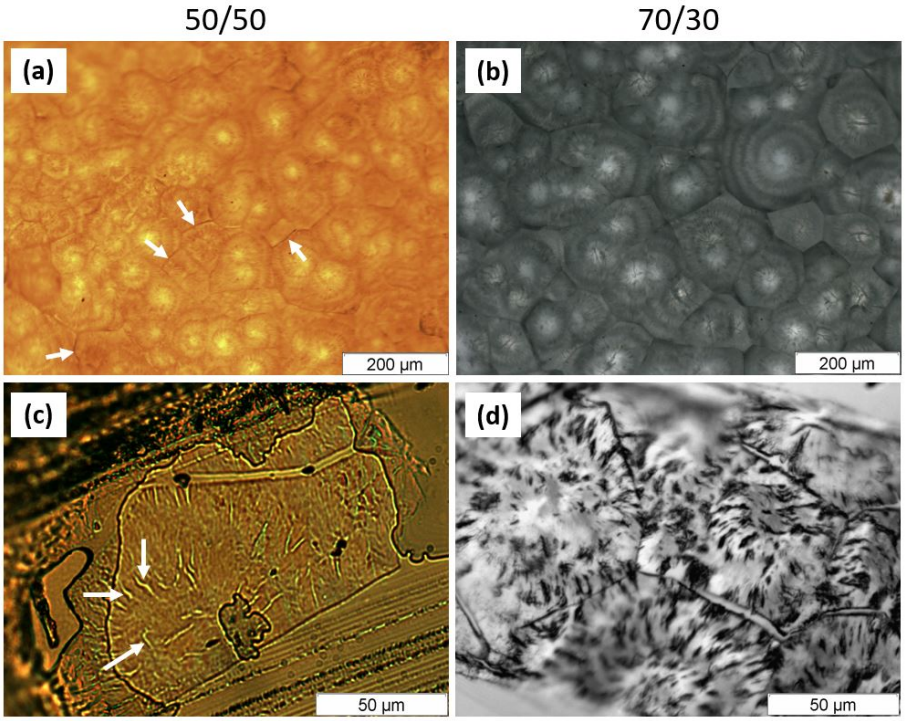

Figure 5.4: POM micrographs of (a) a surface of PLA/PEG 100K 50/50, (b) a surface of PLA/PEG 100K 70/30, (c) a section of PLA/PEG 100K 50/50, and (d) a section of PLA/PEG 100K 70/30. White arrows are discussed in the text.

Blends made with PEG 1M

POM micrographs of PLA/PEG blends made with 50 and 30% of PEG 1M are depicted in Figure 5.5. Images (a) and (b) were taken on the surface of the samples, while images (c) and (d) were taken on the section of the samples. On the surface of PLA/PEG 1M 50/50, shown in Figure 5.5 (a), banded-spherulites are observed as well as interspherulitic black aggregates having a channel shape, some of them being pointed with a white arrow. On the section of this sample, shown in Figure 5.5 (c), elongated holes appear between the spherulites, as pointed with white arrows. Some PEG was located in interspherulitic regions before extraction.

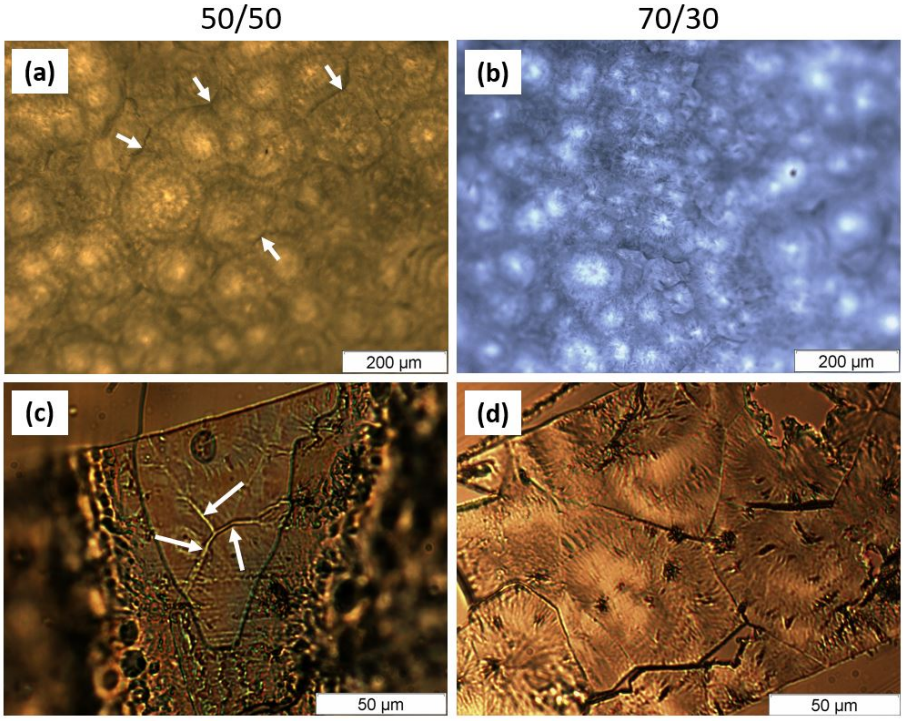

Figure 5.5: POM micrographs of (a) a surface of PLA/PEG 1M 50/50, (b) a surface of PLA/PEG 1M 70/30, (c) a section of PLA/PEG 1M 50/50, and (d) a section of PLA/PEG 1M 70/30. White arrows are discussed in the text.

Figure 5.6 shows a section of the blend PLA/PEG 1M 50/50. It can be observed that this section is very damaged. Many sections were damaged like this one, both for PLA/PEG 100K and 1M 50/50. This confirms interspherulitic segregation of PEG, resulting in mechanically weak interspherulitic cohesion.

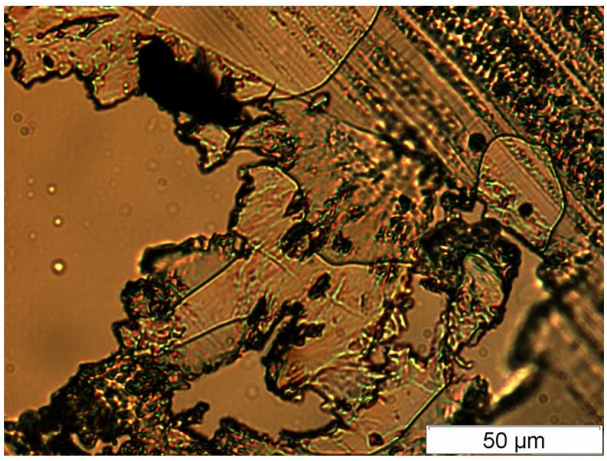

Figure 5.6: POM micrograph of PLA/PEG 1M 50/50, taken on the section of the sample.

5.2.2 Porosity of the blends

In order to observe the porosity inside the samples, SEM micrographs were taken on the slices of the samples with different magnifications. The porous areas correspond to the areas where the PEG was located before extraction.

Blends made with PEG 100K

Figure 5.7 shows SEM micrographs at low magnification. Image (a) presents the blend made with 50 wt% of PEG 100K and image (b) shows the blend made with 30 wt% of PEG 100K.

Size of the spherulites PLA/PEG 100K 50/50 blend presents larger spherulites than PLA/PEG 100K 70/30 blend. The spherulites of the blend with 50% of PEG have a diameter of about 90-110 μm, while the ones of the PLA/PEG 100K 70/30 sample measure about 65-100 μm.

Spatial distribution of the pores When comparing PLA/PEG 100K 50/50 blend, shown in Figure 5.7 (a), and PLA/PEG 100K 70/30 blend, shown in Figure 5.7 (b), it can be observed that when the content of PEG is increased to 50%, the samples are more porous.

In the blend PLA/PEG 100K 50/50, large pores are present at interspherulitic regions. Some of them are so large that they rather form a big hole, separating the spherulites from each other, as shown by the red circle. As there is more PEG in the blend, when the PLA crystallizes, more PEG will inevitably accumulate outside

the spherulites, leading to larger pores after extraction. In PLA/PEG 100K 50/50 blend, more pores are observed inside the spherulites, at interfibrillar regions, than in PLA/PEG 100K 70/30 blend.

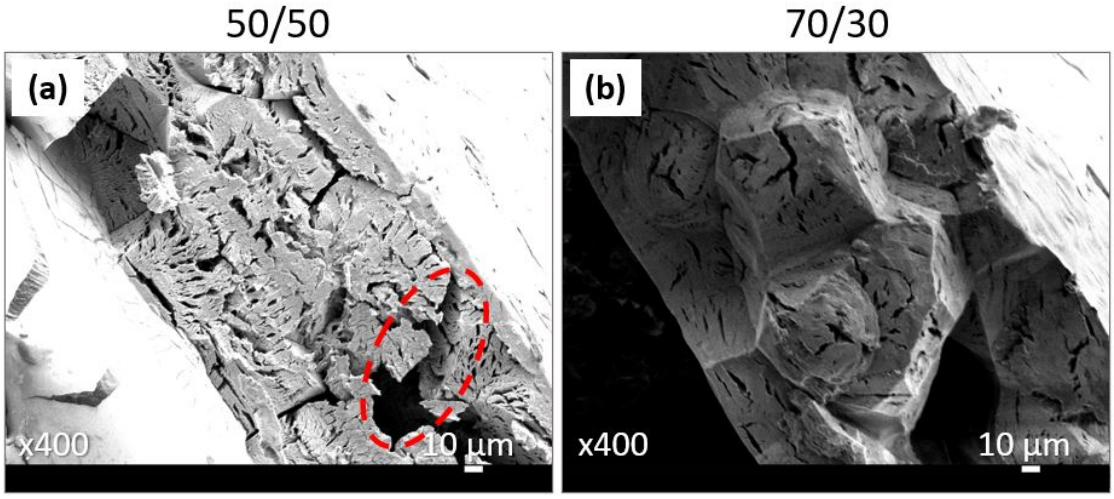

Figure 5.7: SEM micrographs of (a) PLA/PEG 100K 50/50, and (b) PLA/PEG 100K 70/30, taken on the slice of the samples.

Figure 5.8 shows SEM micrographs at higher magnification of PLA/PEG 100K 50/50 blend. It can be observed that the sample is highly porous and that the latter exhibits interfibrillar porosity. The pores located between the fibrils exhibit an elongated shape. Porosity is present all over the sample but is heterogeneous in size. Indeed, some areas present larger pores than others such as the one depicted in Figure 5.8.

Size of the pores The size of the pores was compared for PLA/PEG 100K with a PEG content of 50 and 30%. The size of the intraspherulitic pores was measured on SEM micrographs at different magnifications, depicted in Figure 5.9. For PLA/PEG 100K 50/50, the size of the pores measured on the image taken with a magnification x5,000 ranges from about 1 to 7 μm. The one measured on the image taken with a magnification x22,000 lies between 0.5 and 1.5 μm. There are pores smaller than 0.5 μm and pores larger than 7 μm but the aim is to compare average pore size ranges. When measuring pores in the sample made with 30% of PEG 100K, we find that the pores present the same size on average. The larger pores range from about 1.5 to 6 μm, and the smaller pores measure approximately 0.2 and 1.2 μm. The porosity is heterogeneously distributed in both samples and, as a consequence, the porosity as well as the size of the pores can differ depending

on where the image was taken in the sample, especially at high magnification. This is why we compare the average pore sizes.

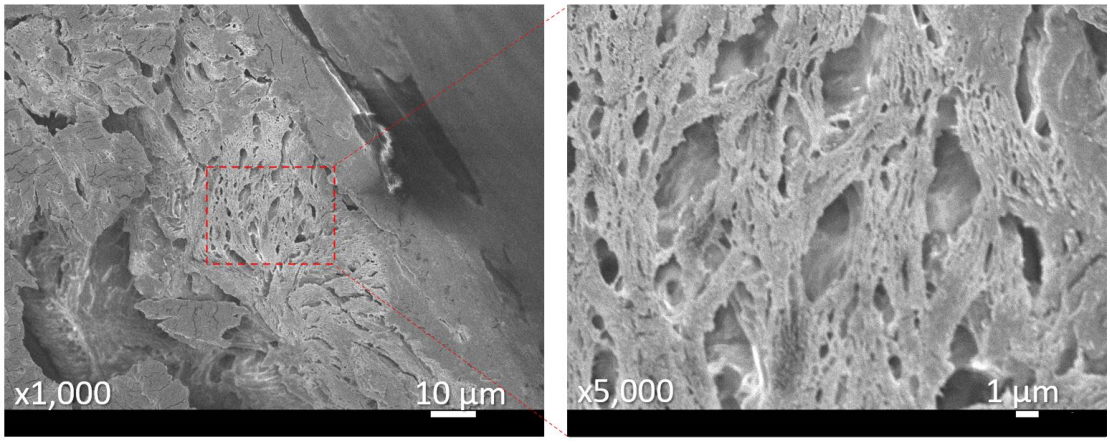

Figure 5.8: SEM micrographs of PLA/PEG 100K 50/50, taken on the slice of the sample.

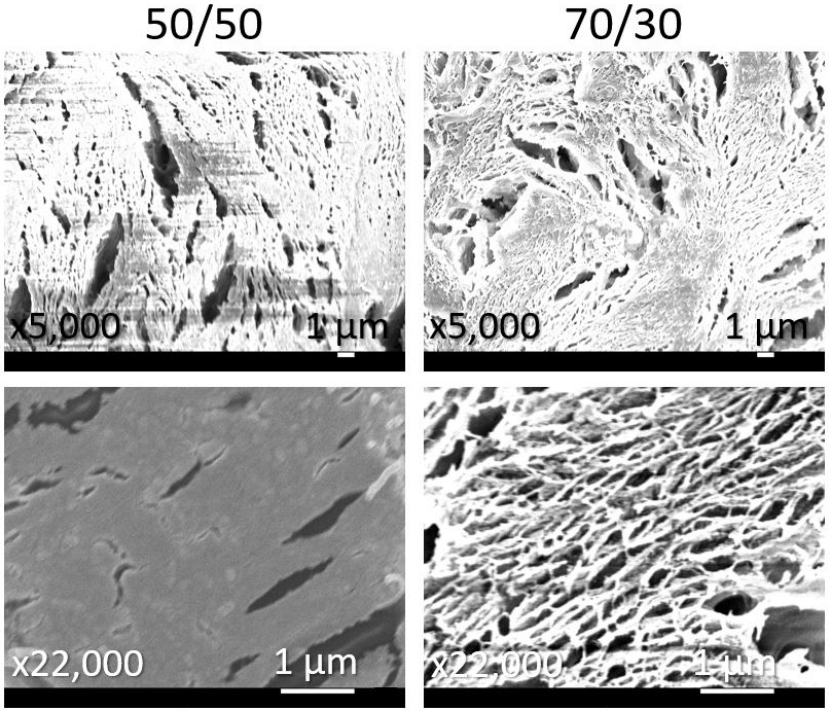

Figure 5.9: SEM micrographs of PLA/PEG 100K 50/50 (*on the left*), and PLA/PEG 100K 70/30 (*on the right)*, taken on the slice of the samples.

Blends made with PEG 1M

Figure 5.10 shows SEM micrographs at low magnification of PLA/PEG blends made with PEG 1M. Images (a) and (b) show the blend made with 50 and 30% of PEG, respectively.

Size of the spherulites PLA/PEG 1M 50/50 presents larger spherulites than PLA/PEG 1M 70/30. The spherulites of the blend with 50% of PEG have a diameter of about 55-95 μm, while the ones of the PLA/PEG 70/30 sample measure about 50-65 μm.

Spatial distribution of the pores The blend made with 50% of PEG 1M, shown in Figure 5.10 (a), exhibits extremely large porosity in the interspherulitic regions, compared to the blend made with only 30% of PEG 1M, shown in Figure 5.10 (b). This porosity is so large that, as for PLA/PEG 100K 50/50, the spherulites seem separated from each other. PLA/PEG 1M 50/50 also exhibits interfibrillar porosity.

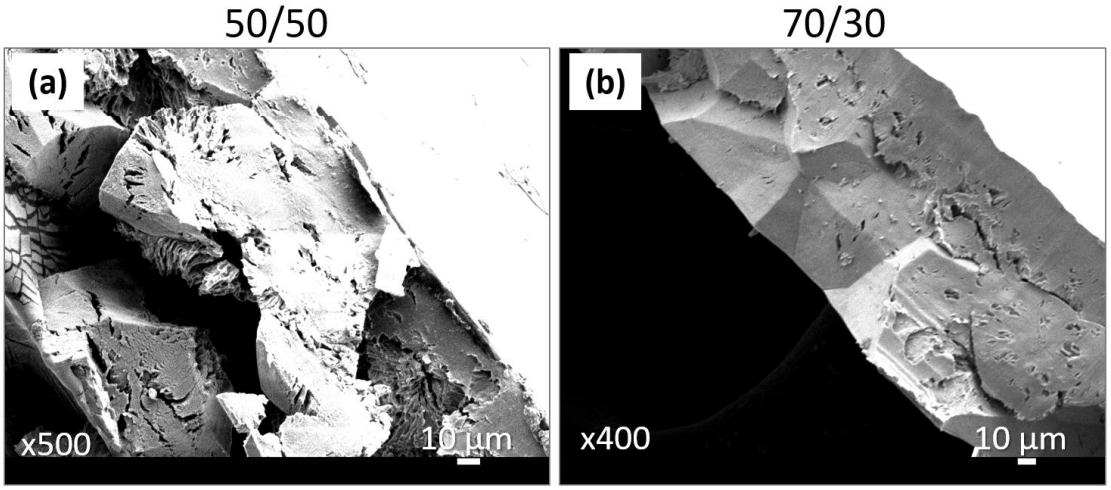

Figure 5.10: SEM micrographs of (a) PLA/PEG 1M 50/50, and (b) PLA/PEG 1M 70/30, taken on the slice of the samples.

Size of the pores Figure 5.11 shows SEM micrographs of PLA/PEG 1M with a PEG content of 50 and 30%, at different magnifications. The size of the pores was measured on these different micrographs to compare the size of the pores between the two different blends. Once again, we only measured the size of the intraspherulitic pores. For PLA/PEG 1M 50/50, the size of the pores measured on

the image with a magnification x5,000 and x22,000 ranges from about 1 to 6 μm, and 0.2 to 1.5 μm, respectively. PLA/PEG 1M 70/30 exhibits pores with a size of about 0.9-2.2 μm for the larger pores, and 0.3-1.5 μm for the smaller ones.

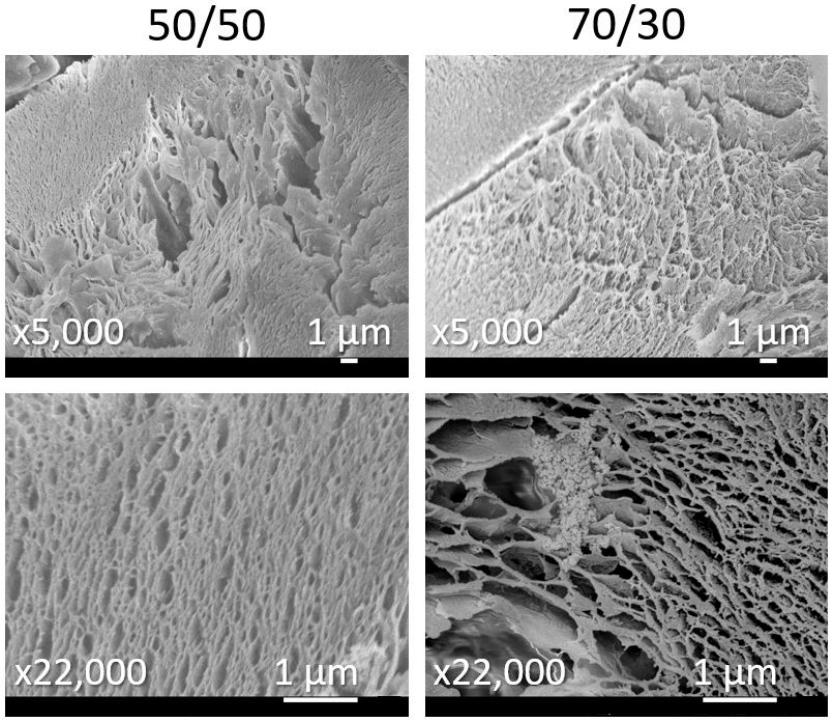

Figure 5.11: SEM micrographs of PLA/PEG 1M 50/50 (*on the left*), and PLA/PEG 1M 70/30 (*on the right)*, taken on the slice of the samples.

The interspherulitic porosity is more important for the blend made with 50% of PEG than for the one made with 30% of PEG, but the intraspherulitic porosity is quite similar for the different PEG contents, for the two studied molar masses. These observations suggest that some PEG is trapped within PLA spherulites (in interfibrillar or interlamellar regions), and that when there is too much PEG, the excess is expelled outside the PLA spherulites, in interspherulitic regions. This explains why the size of the pore is similar in interfibrillar regions for blends made with 30 and 50% of PEG, and why the interspherulitic porosity is, on the contrary, larger for higher PEG contents.

5.3 Effect of PEG molar mass

As previously mentioned, most studies about PLA/PEG blends focus on PEG of small molar mass. In this section, we will analyse the impact of PEG of higher molar mass. PEK 3K will be studied as the smallest molar mass, PEG 100K has a molar mass equivalent to the one of PLA, and PEG 1M has a higher molar mass than PLA. Only samples with a PEG content of 30% are shown and compared.

5.3.1 Morphology of the blends

Figure 5.12 shows POM micrographs of PLA/PEG 70/30 blends made with (a) PEG 3K, (b) PEG 100K, and (c) PEG 1M. The images were taken on the surface of the samples.

On the surfaces of the three samples, we can observe that the spherulites are banded, with bands observed in the spherulites for all different samples. This is due to the helical radial twisting of the lamellae during crystallization, as explained in Chapter 2. The bands observed are due to the birefringence of the crystals (caused by the different refractive indices of the different regions of the polymer material). When polarized light passes through polymer lamellae, it is affected by their crystalline structure and orientation.

Spherulites of PEG 3K are surrounded by black channels, which correspond to porous areas where PEG was located before extraction.

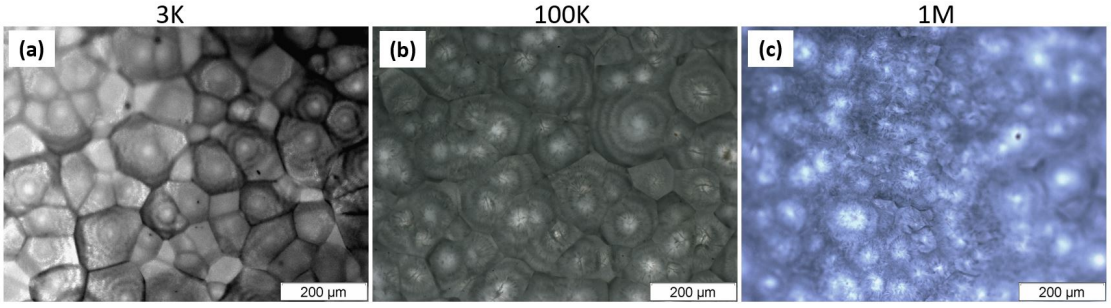

Figure 5.12: POM micrographs of a surface of (a) PLA/PEG 3K 70/30, (b) PLA/PEG 100K 70/30, and (c) PLA/PEG 1M 70/30. Magnification x10.

In order to observe the morphology inside the material, POM micrographs of the sections of the blends PLA/PEG 3K, 100K, and 1M 70/30 are shown in Figure 5.13.

As on the surface, black channels are observed at interspherulitic regions for PEG 3K, shown in Figure 5.13 (a). Some black aggregates are also observed inside

the spherulites, at interfibrillar regions. PEG 3K has a tendency to form many channels in interspherulitic regions and few channels in interfibrillar regions.

Sections of the sample made with PEG 100K, shown in Figure 5.13 (b), exhibit holes between the spherulites and black aggregates between the fibrils. Both holes and black aggregates correspond to porous areas where most of the PEG was located before extraction, leading to empty space, without matter, after PEG extraction. PEG 100K has a tendency to form channels in interspherulitic regions and pockets in interfibrillar regions.

Sections of the sample made with PEG 1M, shown in Figure 5.13 (c), also present inter- and intraspherulitic porosity but the interfibrillar porosity seems to cover less surface than in the blend made with PEG 100K. This is in agreement with the decreased PEG diffusion coefficient as molar mass increases.

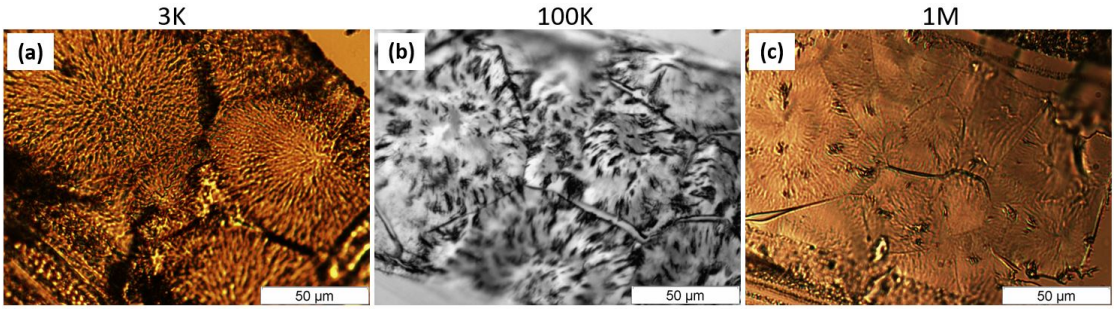

Figure 5.13: POM micrographs of a section of (a) PLA/PEG 3K 70/30, (b) PLA/PEG 100K 70/30, and (c) PLA/PEG 1M 70/30. Magnification x50.

5.3.2 Porosity of the blends

To observe the porosity inside the material and further study the black aggregates observed on POM micrographs, SEM images of the slices of the samples were taken at different magnifications.

Size of the spherulites

In Figure 5.14, SEM micrographs at low magnification of PLA/PEG 3K, 100K, and 1M 70/30 are depicted.

In all pictures, spherulites appear clearly and their shape can be easily observed. The size of the spherulites is about 115-125 μm, 65-100 μm, and 50-65 μm for samples made with PEG 3K, 100K, and 1M, respectively.

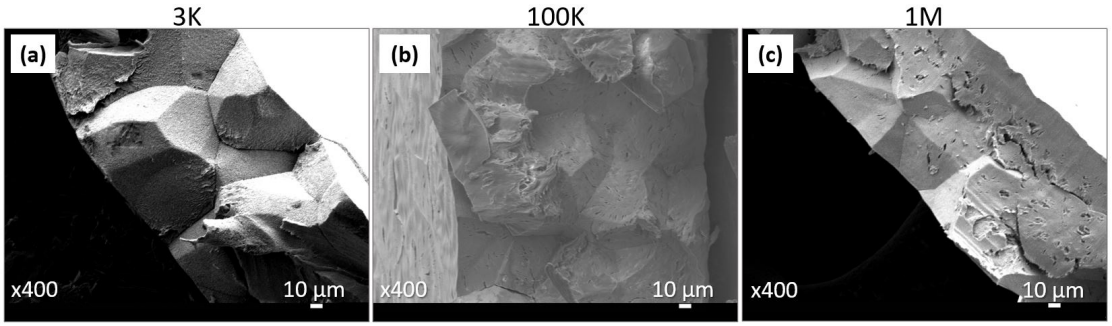

Figure 5.14: SEM micrographs at low magnification of a slice of (a) PLA/PEG 3K 70/30, (b) PLA/PEG 100K 70/30, and (c) PLA/PEG 1M 70/30.

Spatial distribution of the pores

PEG 3K 70/30 SEM micrographs of the slice of PLA/PEG 3K 70/30 are shown in Figure 5.15 at higher magnification. Three spherulites as well as their boundaries appear clearly on the micrograph depicted in Figure 5.15 (b). The spherulites all despite a different intraspherulitic porosity. The most porous zone, shown in Figure 5.15 (a) seems to exhibit an open porosity. Even the least porous zones contain more porous areas as highlighted by the white marks in Figure 5.15 (c). The difference in porosity between the different spherulites can be explained by the fact that the spherulites are oriented differently with respect to the cut. If we cut perpendicularly to the pores, the porosity appears clearly, if we cut parallelly, it will be almost not observable. The sample is also porous in interspherulitic regions.

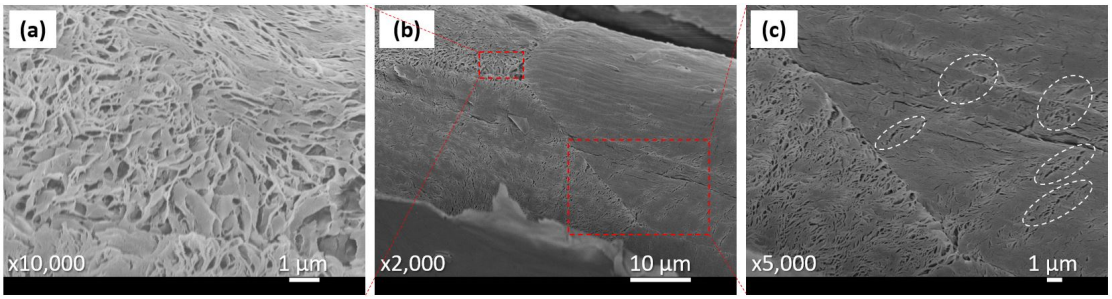

Figure 5.15: SEM micrographs of a slice of PLA/PEG 3K 70/30. (a) Most porous zone (magnification x10,000), (b) overall view (magnification x2,000), and (c) less porous zone (magnification x5,000).

PEG 100K 70/30 Figure 5.16 shows SEM micrographs of the slice of PLA/PEG 100K 70/30. It can be observed that the spherulites present pores between their

fibrils. These pores have an elongated shape. Some of these interfibrillar pores are larger, the PEG has accumulated in the form of pockets between the fibrils, creating these large elongated pores.

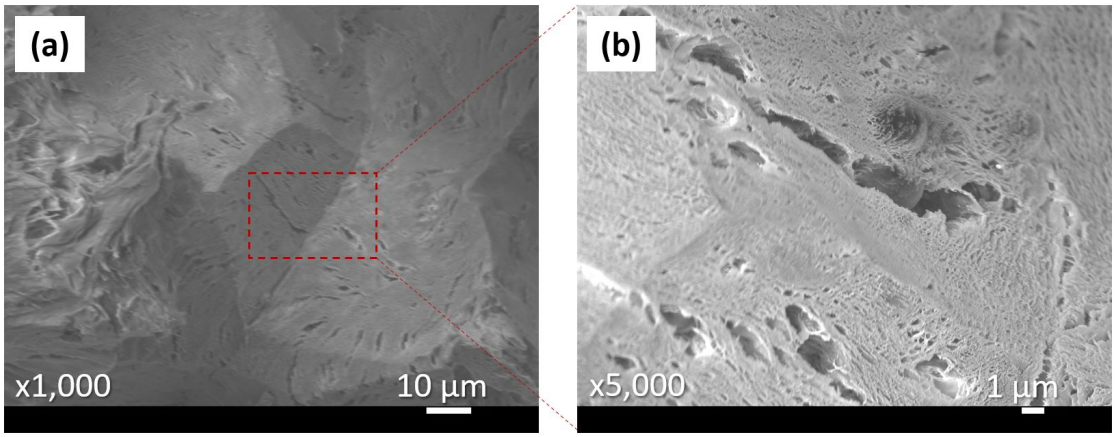

Figure 5.16: SEM micrographs of a slice of PLA/PEG 100K 70/30. (a) Overall view (magnification x1,000), and (b) zoom on interfibrillar porosity (magnification x5,000).

PEG 1M 70/30 SEM micrographs of the slice of PLA/PEG 1M 70/30 are shown in Figure 5.17. Interfibrillar pores can be observed in Figure 5.17 (b). These pores have an elongated shape, like the ones observed on the sample made with PEG 100K. When comparing Figure 5.17 (b) and (c), taken with the same magnification, it can be observed that the porosity is heterogeneously distributed over the blend. The image depicted in Figure 5.17 (b) exhibits a porosity on the order of one micrometer while the image shown in Figure 5.17 (c) has a porosity on the order of 100 nm. It can be explained by the fact that this area was cut inside a spherulite instead of between two spherulites. When cutting the sample with the blade, the cutting is done in a random way. It took place mostly at interspherulitic boundaries because these areas are more fragile, but it can be observed that it also took place inside the spherulites. The cutting may also induce a spreading of the matter which could also explain the difference in porosity over the slice.

Interspherulitic regions In Figure 5.18, SEM micrographs showing an interspherulitic boundary of each sample are depicted. We can observe that with the three different PEG molar masses, there is an important porosity between two spherulites. The latter is however smaller for PLA/PEG 1M. Indeed, this blend only shows some elongated pores at interspherulitic regions while PLA/PEG 3K and 100K present long empty channels between two spherulites.

In Figure 5.18 (a) and (b), we can observe the two different orientations of the lamellae. On the left of the images, the orientation is edge-on. The pores were cut perpendicularly and appear clearly on the image. On the right of the images, the orientation is flat-on. The pores were cut parallelly and are almost not visible.

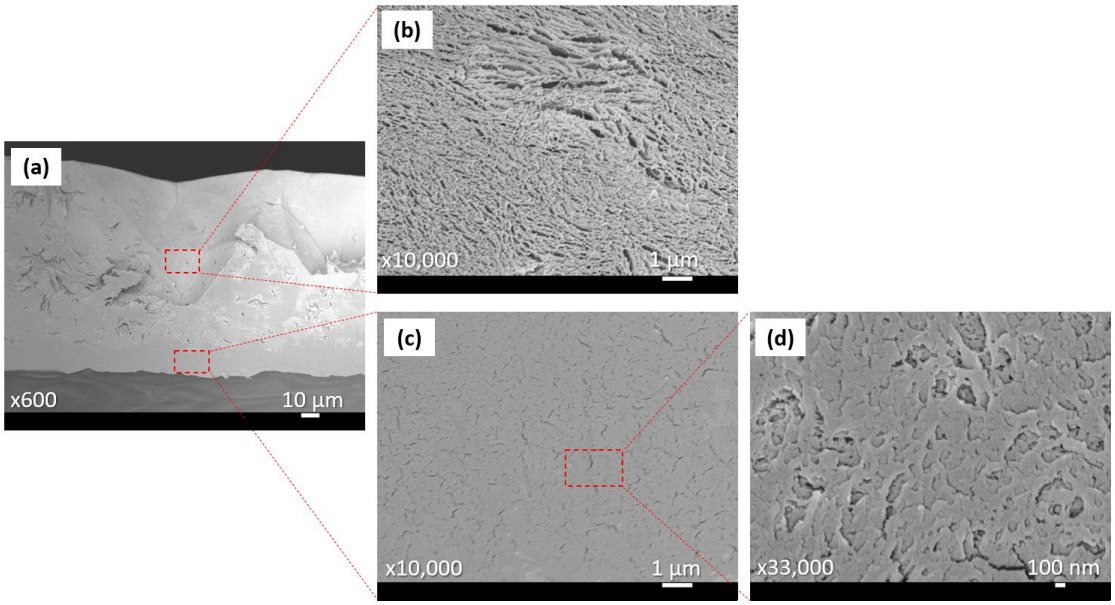

Figure 5.17: SEM micrographs of a slice of PLA/PEG 1M 70/30. (a) Overall view (magnification x600), (b) more porous zone (magnification x10,000), (c) least porous zone (magnification x10,000), and (d) zoom of the least porous zone (magnification x33,000).

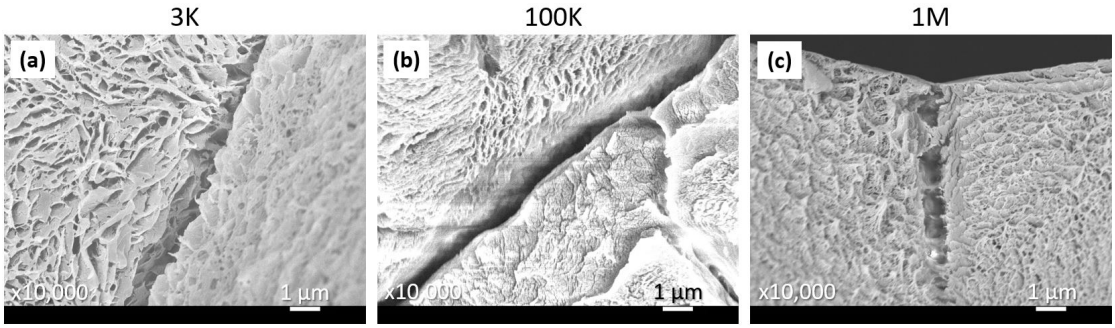

Figure 5.18: SEM micrographs of an interspherulitic boundary, taken on a slice of (a) PLA/PEG 3K, (b) PLA/PEG 100K, and (c) PLA/PEG 1M 70/30. Magnification x10,000.

Size of the pores

The size of the pores was measured on the three samples at different magnifications. SEM micrographs are depicted in Figure 5.19. The first, second, and third columns represent images that were taken on samples made with PEG 3K, 100K, and 1M, respectively (with a content of 30% of PEG). The rows represent three different magnifications. The measurements were taken at random locations on the samples, so the images shown for each sample at different magnifications were not especially taken at the same location in the sample.

For each sample, we find three different orders of magnitude concerning the size of the pores as shown in Table 5.1. It can be observed that, for each sample, the different pore sizes are in the same ranges. It is important to keep in mind that, as the pores are heterogeneously distributed across the sample, depending on the location in the sample where the pores were measured, the pore size may be a bit different. Therefore, even if some pores may seem larger for some samples, the values are close enough so that we can consider them to be in the same range.

When observing Figure 5.19, we can see that the pores exhibit the same elongated shape and distribution for all samples at magnification x22,000 (second row). However, with a magnification x5,000 (first row), we observe larger interfibrillar pores on PLA/PEG 100K slice. Large bundles of PEG appear to accumulate between the fibrils during crystallization, leaving large, somewhat elongated pores after PEG extraction. The same tendency was observed in Figure 5.16. When the magnification is increased to x50,000 (third row), one could believe that the blend made with PEG 3K exhibits larger porosity. However, as previously said, the porosity is heterogeneously distributed and depends on the location in the sample, especially at higher magnification. This is why the apparent difference in pore size on the images is not relevant.

Table 5.1: Pore size of PLA/PEG 3K, 100K, and 1M 70/30.

	x5,000	**x22,000**	**x50,000**
PEG 3K	0.5-1.5 μm	0.5-1.15 μm	65-650 nm
PEG 100K	0.65-4.95 μm	0.2-1.2 μm	75-400 nm
PEG 1M	0.55-3.55 μm	0.3-1.5 μm	170-270 nm

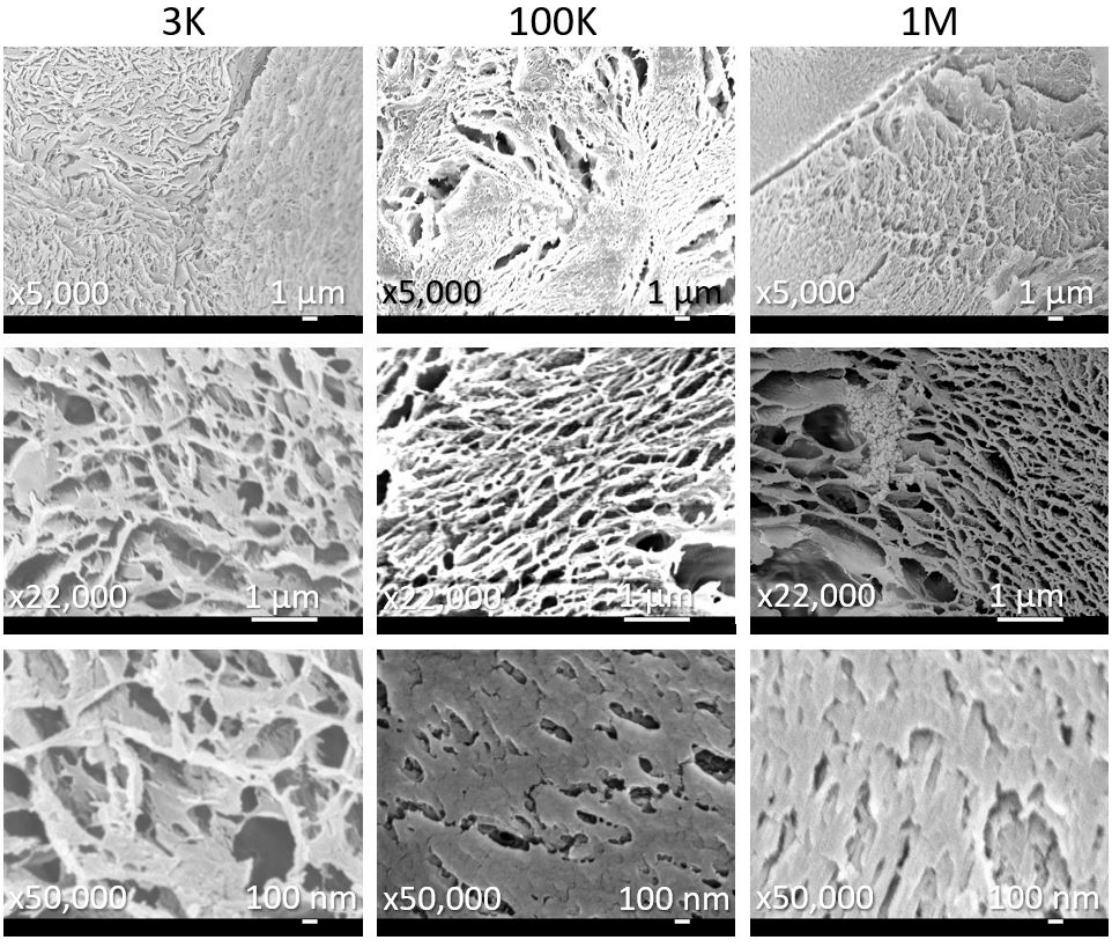

Figure 5.19: SEM micrographs of a slice of PLA/PEG 3K, 100K, and 1M 70/30, taken at different magnifications (x5,000; x22,000; and x50,000).

5.3.3 Morphology and porosity at different depths inside the material

In order to observe the morphology and porosity at different depths inside the material, we observed the blend PLA/PEG 100K 70/30 with CLSM. The sample was colored with rhodamine.

Figure 5.20 shows micrographs taken with CLSM. The three images were taken at the same location in the sample but at different depths. The first image, on the left, is closer to the surface facing the laser source and the following images were taken by going down in the sample.

The shape of different spherulites clearly appears on the images. The bands of

the spherulites are observed on the first two images, some of them pointed with white arrows. These bands were already observed on the surface with POM, and we can see that they are also present inside the material.

The fibrils of the spherulites are also clearly observed, starting from the center of the spherulite and extending to the edge of it. Some fibrils are surrounded by white marks. Black channels are observed at interspherulitic regions. They appear in a much more marked way than with POM because we can see that the rhodamine has been deposited around the holes, where there was matter (the holes therefore appear very black).

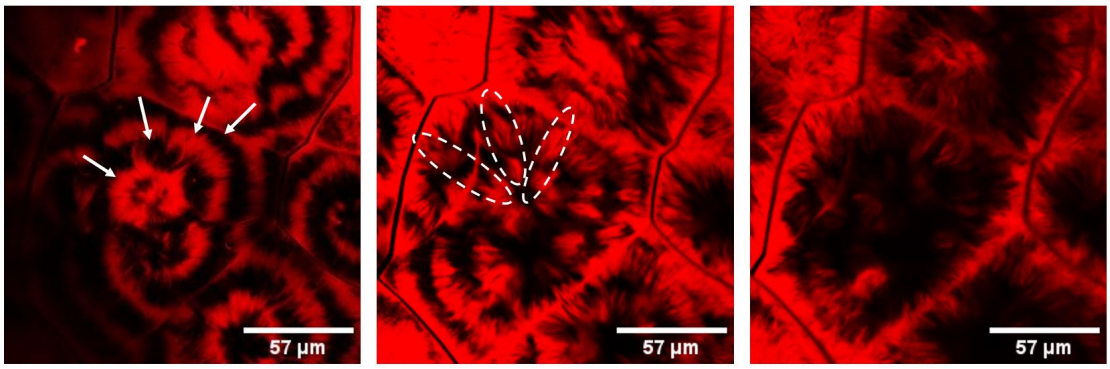

Figure 5.20: CLSM micrographs of the blend PLA/PEG 100K 70/30 coated with rhodamine. Magnification x63. White arrows are discussed in the text.

Micrographs depicted in Figure 5.21 were taken on the same sample (PLA/PEG 100K 70/30) at higher magnification in order to observe an interspherulitic crack. We observe once again that the crack appears black and the edge of the spherulites next to the crack appears red across the entire sample. On the first two images, the bands and the fibrils are once again observed. Some bands are pointed with a white arrow and some fibrils are surrounded by white marks.

3D images were reconstructed with the confocal microscope and are depicted in Figure 5.22. When observing these 3D images, it is possible to enter layer by layer to see the evolution of the morphology inside the material.

In Figure 5.22 (a), the bands appear in 3D and the interspherulitic boundaries are clearly visible. In these images, colors are a function of height. Red areas are the highest and blue areas the lowest in the sample. We can observe that the surface is not flat, on the contrary, it appears rough and raised. When observing below the surface, we can see that color appears beneath the outermost surfaces of the spherulites. Below the center of the spherulites (which appears red on the surface), on the other hand, we see no color at all, the image is black. This means that

scattering of the incoming light and/or of the fluorescence prevents the fluorescent light to reach the detector. We thus cannot observe these regions.

As observed in Figure 5.22 (b), by entering the sample layer by layer, we see several elongated pores, some of them pointed with white arrows. Some pores remain over several layers because they are deeper, others appear less deeply through the material. In any case, pores are present in each layer of the sample and are mostly located between the fibrils, as observed on SEM micrographs for samples made with 30% of PEG 100K.

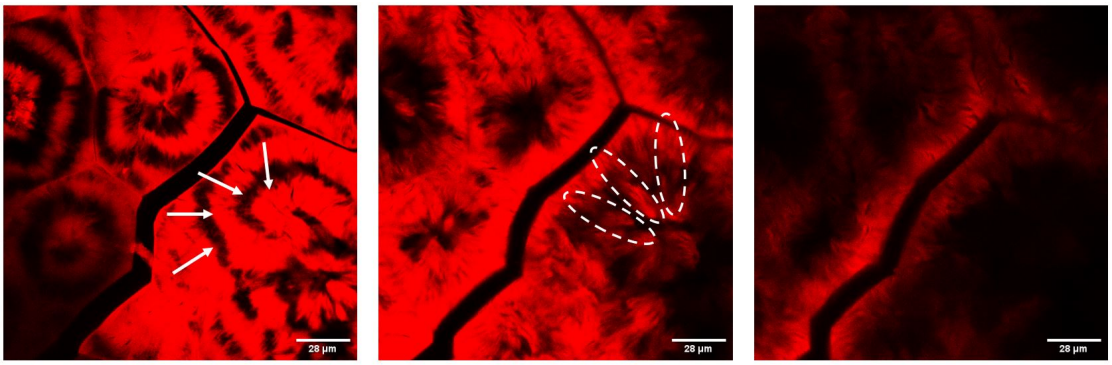

Figure 5.21: CLSM micrographs of a crack of the blend PLA/PEG 100K 70/30 coated with rhodamine. Scale bar represents 28 μm. White arrows are discussed in the text.

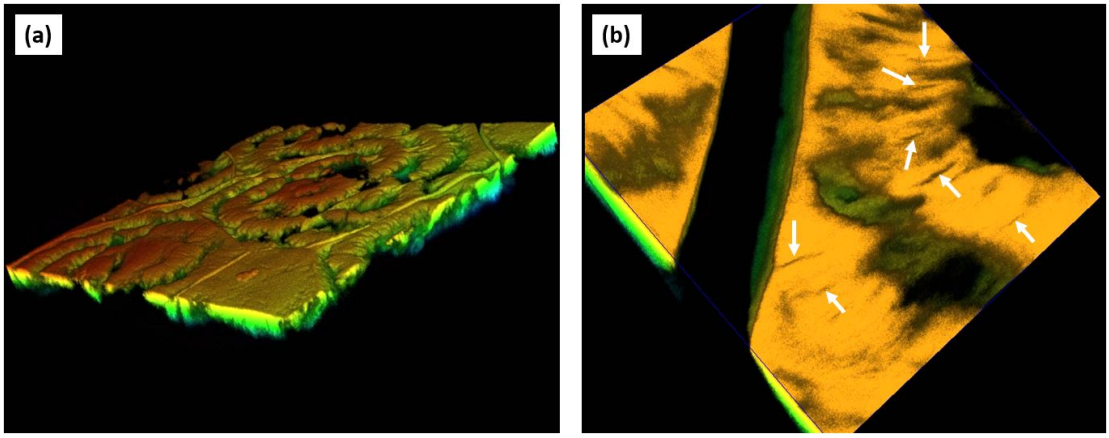

Figure 5.22: CLSM 3D images of the blend PLA/PEG 100K 70/30 coated with rhodamine, (a) the top of the 3D image corresponds to the surface of the sample, and spherulites can be observed, and (b) the top of the 3D image corresponds to a layer inside the material, and a crack as well as some pores can be observed.

There is however a problem when imaging crystallized samples with CLSM. Indeed, some areas that appear dark on the images are not holes, because these areas do not correspond to the pores observed on SEM images. We then have to observe the samples while keeping in mind that black areas are not necessarily holes. These black areas in the images can be explained by various phenomena: rhodamine has not deposited in these areas, or the incident light produced by the laser is not reaching these areas, or the fluorescent light emitted by the sample does not emerge from the sample and does not reach the detector. The most likely hypothesis is that fluorescent light does not emerge from the sample at certain points and does not reach the detector, as it emits little and is recaptured by the sample. Indeed, the incident light produced by the laser is very strong, and it is unlikely that it will not be able to pass through these polymer samples. Also, if we look at the different CLSM images shown in Figures 5.20 and 5.21, we can see that the rhodamine appears to diffuse everywhere at each depth, and appears to diffuse in depth as well. The porosity would therefore be open (allowing rhodamine to diffuse through the sample), and there is no reason why deeper into the sample, the porosity would be different from anywhere else inside the material. Moreover, to color the sample, it was first immersed in rhodamine, which was therefore able to enter the sample from all surfaces.

It was observed that we can see the contrast between holes and matter in an easier way near cracks. Indeed, as shown in Figure 5.22 (b), porosity is easily observed near cracks and it correspond to the porosity observed with SEM. It is then better to observe the porosity of the sample near cracks, when using confocal microscopy with fluorescence.

5.4 General discussion

Effect of PEG concentration

Size of the spherulites From the results presented above, it can be concluded that the content of PEG in PLA/PEG blends has an impact on the blend properties. Regarding PLA/PEG blends with 50 and 30% of PEG, we observed that, for both studied molar masses (PEG 100K and 1M), the spherulites are bigger but less numerous with 50% of PEG, as observed in Figures 5.7 and 5.10. The addition of PEG increases PLA crystallization rate. Indeed, PEG is less viscous that PLA and so decreases blend viscosity and PLA chain entanglements, allowing PLA chains to move in an easier way. The number of nucleation sites decreases with increasing PEG content as PEG cannot act as heterogeneous nucleation site for PLA [51]. Indeed, as heterogeneous nucleation sites may be present in PLA but not in PEG, by diluting PLA with PEG, nucleation density could decrease with the addition of PEG. As nucleation density is lower with the addition of PEG, the spherulites are less numerous and bigger. Moreover, when the spherulites are smaller, the surface-to-volume ratio is higher, leading to more interspherulitic regions. We can expect more PEG in interspherulitic regions and so more interspherulitic porosity after PEG extraction.

Porosity PLA/PEG 50/50 blends and PLA/PEG 70/30 blends present a similar interfibrillar porosity, for the two molar masses studied, as observed in Figures 5.9 and 5.11. The size of the interfibrillar pores was on the same order of magnitude for both PEG contents. However, blends made with a PLA/PEG composition of 50/50 exhibit a larger interspherulitic porosity than the ones made with a 70/30 composition, despite the fact that they have larger spherulites, as observed in Figures 5.7 and 5.10. In PLA/PEG 50/50 blends, between the spherulites, some holes are so large that the spherulites are separated from each others. The material could lack cohesion and be too prone to failure.

When the PEG content is increased in the blend, more PEG will accumulate between the spherulites during PLA crystallization but the amount of interfibrillar PEG is similar. As previously mentioned, these observations suggest that a part of the PEG is trapped inside the spherulites and that when the PEG content is increased above a critical value, the excess is expelled from spherulites and locate in interspherulitic regions. As the porosity is induced via PEG extraction, larger pores will be created at interspherulitic regions for PLA/PEG 50/50 blends, and pores of the same size on average will be created at interfibrillar regions for PLA/PEG 50/50 and PLA/PEG 70/30 blends.

The interspherulitic porosity of PLA/PEG 50/50 blends is too high and makes

the material too fragile. The extraction of PEG allows to induce microporosity in the material. As PEG diffuses outwards the spherulites, it can segregate between the spherulites, between the fibrils or between the lamellae. When PEG content is to high, the induced porosity can become a problem. Indeed, if too much matter is extracted from the same place in the material, the material can lack cohesion. That is what happens when the initial PEG content is 50% because too much PEG accumulates in interspherulitic regions, leaving large empty spaces after extraction. We observed on SEM images that big holes were standing at interspherulitic regions and we observed on POM images that the material is so fragile that several sections broke by cutting them with the microtome. The most promising PEG content for PLA/PEG blends to be used as biomaterials is therefore 30 wt%.

Effect of PEG molar mass

Size of the spherulites It was observed in Figure 5.14 that, the higher the PEG molar mass, the smaller and more numerous the PLA spherulites and vice versa. It is again explained by the viscosity of PEG. PEG is less viscous for smaller molar masses, like PEG 3K, and the spherulites of PLA grow at a faster rate during PLA crystallization, leading to larger spherulites. When the molar mass is higher, like PEG 1M, and the spherulites are smaller, more PEG could be located in interspherulitic regions after crystallization.

Spatial distribution of the pores The spatial distribution of porosity changes from one blend to another, depending on the molar mass. Indeed, the porosity was induced via PEG extraction and is then related to areas where PEG was located after crystallization of the blends. As explained in Chapter 2, the areas where PEG will segregate during crystallization depends on its diffusion coefficient relative to the radial growth rate of PLA spherulites. If the diffusion coefficient of PEG is higher than the radial growth rate of PLA spherulites, PEG will have time to diffuse out of the spherulites and will segregate between the spherulites, in interspherulitic regions. On the contrary, if the radial growth rate of PLA spherulites is higher, PEG will be retained inside the spherulites and will locate mainly either between the fibrils and/or between the lamellae.

As observed in Figures 5.15 and 5.18, samples made with PEG 3K present more interspherulitic porosity because, as the molar mass of PEG is smaller, it is less viscous and it diffuses at a faster rate outside the spherulites. This phenomenon explains why it was impossible to obtain a film of sufficient quality for the PLA/PEG 3K 50/50 blend. PEG 3K also presents some interfibrillar pores. Samples made with PEG 100K present large elongated pores at interfibrillar regions as observed in Figure 5.16, indicating that PEG accumulated as large pockets between the fibrils during PLA crystallization. Indeed, during PLA crystallization, PEG diffuses

and gets trapped between PLA fibrils, whereas it was diffusing outwards from the spherulites. PEG will therefore be present in the form of elongated pockets between PLA fibrils, giving way to elongated pores after extraction. As the PLA used in these experiments also has a molar mass of 100 000 g/mol, the two polymers have an equivalent molar mass. The PEG starts diffusing outside the spherulites but as PLA spherulites grow at the same time, elongated regions of PEG are stuck between the fibrils of the spherulites, leaving elongated interfibrillar pores after PEG extraction. PEG 100K also presents an important interspherulitic porosity, in the shape of channels, as observed in Figure 5.18. PEG 1M presents smaller interspherulitic pores that PEG 3K and 100K. Indeed, PEG 1M diffuses at a slower rate because the molar mass and so the viscosity is higher. The radial growth rate of PLA spherulites is higher than the diffusion coefficient of PEG, so more PEG is trapped inside the spherulites and less PEG accumulates in interspherulitic regions. As observed in Figure 5.17, PEG 1M also presents elongated pores in interfibrillar regions.

Size of the pores In this study, we fabricated samples with microporosity induced by the extraction of PEG in different PLA/PEG blends. As observed in Figure 5.19, the largest pores obtained are about 5 μm in size. Interconnected micropores in the scaffold should increase mass transfer, thereby increasing intercellular communication in the tissue-engineered construct, leading to an improved formation of 3D tissues [78]. As explained in Chapter 2, pores of 5 μm allow neovascularization and may allow fibroblast ingrowth. Fibroblast ingrowth requires pores with a size ranging from 5 to 15 μm. However, the pores of the blends are to small to induce the regeneration of certain tissues such as bone, they are also to small for the ingrowth of certain types of cells such as hepatocytes. In order for the scaffold to properly perform its functions, including promotion of cell-biomaterial attachment, is should contain both micro- and macroporosity. The microporosity was induced via PEG extraction, the macroporosity can be created via 3D-printing. When a scaffold is implanted in a patient, the interconnected porosity also increases the contact surface of the scaffold with biological fluids, increasing the water absorption of the scaffold and increasing its degradation rate. As PLA degrades too slowly, increasing porosity to enhance the degradation rate is beneficial in the context of tissue-engineered constructs.

From these results, we can argue that PLA/PEG blends created with extraction of PEG 3K are less favorable to be used as biomaterials. Indeed, more PEG diffuses outside the spherulites during crystallization and segregates between the spherulites, where it crystallizes in turn if the temperature is reduced to its crystallization temperature, because it is present at a sufficiently pure concentration. When the PEG is extracted, pores will be located mostly between the spherulites and not

inside them. The porosity will therefore be less homogeneously distributed. As biomaterials require an open porosity, blends made with PEG 3K are less promising. Moreover, samples made from PEG 3K are more fragile. Only we have larger spherulites, which can facilitate the propagation of cracks through the material via the spherulite boundaries. Also, there is more PEG in the interspherulitic regions and therefore more porosity after extraction, which also makes the sample more brittle.

In blends made with the extraction of PEG 100K and 1M, on the contrary, there are pores located between the fibrils of the spherulites. The pores have an elongated shape for both samples but they are larger for samples made with PEG 100K. In this sample, PEG accumulates as pockets between the PLA fibrils during crystallization, leaving large elongated pores after PEG extraction. Both, PLA/PEG 100K and 1M also present pores in interspherulitic regions, in smaller quantities than PEG 3K. The pores are more homogeneously distributed and therefore the porosity will be more likely to be open throughout the material. The PLA/PEG 100K 70/30 blend does indeed exhibit open porosity, as shown by the CLSM images: we can see that the rhodamine has diffused into the sample.

Chapter 6

Conclusion

The aim of this work was to assess the porosity of PLA/PEG blends to be used as scaffold biomaterials. Indeed, a scaffold should provide a tradeoff between porosity, which allows the diffusion of nutrients and cells, and mechanical properties which provide good mechanical support for cells. The porosity was induced by extracting the PEG phase from the blends. Two main parameters, influencing blend porosity, were studied: PEG content in the blend and PEG molar mass. The morphology and the porosity of the blends were studied inside the material after PEG extraction using POM, SEM, and CLSM.

The effect of PEG content was studied on two different compositions: 50 wt%, and 30 wt% of PEG. It was observed that the samples made with the two different concentrations exhibit a similar intraspherulitic porosity but a different interspherulitic porosity. Indeed, while PLA/PEG 70/30 blends present interspherulitic pores having the shape of narrow channels or elongated pores, PLA/PEG 50/50 blends present large holes at interspherulitic regions, separating the spherulites from each others. The blends made with 50% of PEG are thus too brittle and too prone to failure. As the interfibrillar porosity is similar for the two different PEG contents and the PLA/PEG 50/50 blends are too fragile, it was concluded that blends made with a PEG content of 30% are more promising to create porous scaffolds.

Three different PEG molar masses were studied: PEG 3K, PEG 100K, and PEG 1M. The samples made with PEG 3K exhibit more interspherulitic porosity because PEG 3K diffuses at a faster rate outwards from spherulites during PLA crystallization. The samples made with PEG 100K and PEG 1M, on the other hand, present more interfibrillar porosity, the pores have a large elongated shape. The samples made with PEG 100K and 1M also present interspherulitic porosity, but this is less significant than in samples made with PEG 3K. As samples made

with PEG 3K are more brittle, due to their large interspherulitic porosity and reduced number of chains connecting two neighbouring PEG lamellar crystals, it was concluded that this molar mass is less promising to be used for the production of scaffold biomaterials. PEG 100K and 1M, on the other hand, seem both promising. Confocal microscopy confirmed that the PLA/PEG 100K 70/30 blend exhibits an interconnected porosity which would allow the diffusion of nutrients and cells.

To better characterize the porosity, additional measurements could be performed. The total porosity of the blends could be evaluated based on SEM images. The ratio between the empty volume (the pores) and the total volume of the material (filled + empty volume) could be computed. The full volume appears bright while the pores are darker, on SEM images. However, as the porosity is in 3D but the SEM images are in 2D, this method would only give a rough estimate of porosity. Other measurement methods could be used to characterize the porosity more precisely. For example, mercury intrusion porosimetry (MIP) allows to characterize the pore size distribution as well as the total porosity. It could be very useful to complete our measurements. Indeed, we have already assessed the spatial distribution of the pores. Gas adsorption techniques such as nitrogen or carbon dioxide adsorption allow to characterize the surface area and porosity.

In order to study the interconnected porosity in 3D, a more suitable means of imaging crystallized polymers than confocal microscopy could be micro-computed tomography (μCT). This imaging technique works with X-rays instead of light and is non-destructive. X-rays pass through much more material than light, including crystalline polymers. Kuterbekov *et al.* [79] obtained μCT-reconstructed 3D images of a blend of PLLA/PEG with 30 wt% of PLLA and 70 wt% of PEG. The PEG was extracted from the sample. The porosity was easily observed on the μCT-reconstructed images.

The extraction of PEG allowed to induce microporosity, having a size ranging from a few tens of nanometers to approximately 5 μm. In order to produce scaffolds exhibiting both micro- and macroporosity, the latter could be induced via 3D-printing. 3D-printing allows to create pores of several tens of micrometers and can also be used to create a scaffold whose shape is adapted to that of the patient tissue it replaces. To take our research a step further, the mechanical properties could be tested on the 3D-printed samples, for example, via tensile tests. Indeed, the mechanical properties were not tested in this work yet they play a crucial role in cell support and structural maintenance.

In order to further modify and better control the porosity of the blends, some methods could be used. Other PEG contents and PEG molar masses could be studied. The blends made with 50% of PEG already exhibit too large interspherulitic porosity; therefore, preparing blends with more PEG is not relevant. Making blends

with less than 30% of PEG is not interesting because these blends would just exhibit less porosity than PLA/PEG 70/30 blends, but it could be interesting to try an intermediate PEG content, for example 40%. It could also be interesting to study a wider range of PEG molar masses to modulate the porosity. Moreover, in order to induce a larger porosity within the scaffold, porogen materials could be added to the blends, and then removed, like the PEG phase, to create pores. Combining 3D-printing with porogen materials could allow to control the pore size, shape, and distribution within the printed scaffold, as well as the shape of the scaffold. The porogen materials used would have to be carefully selected.

In addition to the mechanical properties, the biocompatibility of the samples can be investigated, biocompatibility being essential for the fabrication of new tissue. To do so, cells can be cultured on the scaffolds to assess cell adhesion, proliferation, and differentiation. The viability of cells could be evaluated using cell fluorescent staining assay, for example. Depending on the tissue we aim to replace, the cultured cell type will be different.

The degradation rate of the scaffolds can also be investigated, for example, by immersing the scaffold in simulated body fluid (SBF). The weight loss can be computed in order to quantify the degradation rate.

Once all the properties have been assessed, and if these ones match the properties required for a tissue engineering scaffold, the next steps will be to test these scaffolds *in vivo* using animal models. The ultimate goal is to one day be able to use these scaffolds for clinical purposes, and to use them to repair patient tissue.

Bibliography

[1] P. K. Chandra, S. Soker, and A. Atala. "Chapter 1 - Tissue engineering: current status and future perspectives". In: *Principles of tissue engineering*. Ed. by R. Lanza et al. London: Academic press, 2020, 1–35. DOI: 10.1016/B978-0-12-818422-6.00004-6.

[2] F. J. O'Brien. "Biomaterials & scaffolds for tissue engineering". *Materials today* 14 (2011), 88–95. DOI: 10.1016/S1369-7021(11)70058-X.

[3] L. Lu and A. G. Mikos. "The importance of new processing techniques in tissue engineering". *MRS bulletin* 21 (1996), 28–32. DOI: 10.1557/S088376940003181X.

[4] E. M. Saffer, G. N. Tew, and S. R. Bhatia. "Poly(lactic acid)-poly(ethylene oxide) block copolymers: new directions in self-assembly and biomedical applications". *Current medicinal chemistry* 18 (2011), 5676–5686. DOI: 10.2174/092986711798347324.

[5] H. Long et al. "Effect of polyethylene glycol on mechanical properties of bamboo fiber-reinforced polylactic acid composites". *Journal of applied polymer science* 136 (2019), 47709. DOI: 10.1002/app.47709.

[6] M. S. Singhvi, S. S. Zinjarde, and D. V. Gokhale. "Polylactic acid: synthesis and biomedical applications". *Journal of applied microbiology* 127 (2019), 1612–1626. DOI: 10.1111/jam.14290.

[7] K. Hamad et al. "Properties and medical applications of polylactic acid: A review". *Express polymer letters* 9 (2015), 435–455. DOI: 10.3144/expresspolymlett.2015.42.

[8] M. Murariu and P. Dubois. "PLA composites: From production to properties". *Advanced drug delivery reviews* 107 (2016), 17–46. DOI: 10.1016/j.addr.2016.04.003.

[9] S. Farah, D. G. Anderson, and R. Langer. "Physical and mechanical properties of PLA, and their functions in widespread applications—A comprehensive review". *Advanced drug delivery reviews* 107 (2016), 367–392. DOI: 10.1016/j.addr.2016.06.012.

[10] R. Scaffaro et al. “Preparation of three-layered porous PLA/PEG scaffold: Relationship between morphology, mechanical behavior and cell permeability”. *Journal of the mechanical behavior of biomedical materials* 54 (2016), 8–20. DOI: 10.1016/j.jmbbm.2015.08.033.

[11] M. A. Ghalia and Y. Dahman. “Fabrication and enhanced mechanical properties of porous PLA/PEG copolymer reinforced with bacterial cellulose nanofibers for soft tissue engineering applications”. *Polymer testing* 61 (2017), 114–131. DOI: 10.1016/j.polymertesting.2017.05.016.

[12] M. Jonoobi et al. “Mechanical properties of cellulose nanofiber (CNF) reinforced polylactic acid (PLA) prepared by twin screw extrusion”. *Composites science and technology* 70 (2010), 1742–1747. DOI: 10.1016/j.compscitech.2010.07.005.

[13] B. Y. Chen et al. “Fabrication of polylactic acid/polyethylene glycol (PLA/PEG) porous scaffold by supercritical CO2 foaming and particle leaching”. *Polymer engineering and science* 55 (2015), 1339–1348. DOI: 10.1002/pen.24073.

[14] T. Serra et al. “Relevance of PEG in PLA-based blends for tissue engineering 3D-printed scaffolds”. *Materials science and engineering: C* 38 (2014), 55–62. DOI: 10.1016/j.msec.2014.01.003.

[15] B. Bhaskar et al. “Composite porous scaffold of PEG/PLA support improved bone matrix deposition in vitro compared to PLA-only scaffolds”. *Journal of biomedical materials research - Part A* 106 (2018), 1334–1340. DOI: 10.1002/jbm.a.36336.

[16] M. A. Elsawy et al. “Hydrolytic degradation of polylactic acid (PLA) and its composites”. *Renewable and sustainable energy reviews* 79 (2017), 1346–1352. DOI: 10.1016/j.rser.2017.05.143.

[17] D. G. A. M. Bianchetti et al. “D-lactic acidosis in humans: systematic literature review”. *Pediatric nephrology* 33 (2018), 673–681. DOI: 10.1007/s00467-017-3844-8.

[18] S. Salehi et al. “The effect of polyethylene glycol on printability, physical and mechanical properties and osteogenic potential of 3D-printed poly(L-lactic acid)/polyethylene glycol scaffold for bone tissue engineering”. *International journal of biological macromolecules* 221 (2022), 1325–1334. DOI: 10.1016/j.ijbiomac.2022.09.027.

[19] Z. U. Arif et al. “Recent advances in 3D-printed polylactide and polycaprolactone-based biomaterials for tissue engineering applications”. *International journal of biological macromolecules* 218 (2022), 930–968. DOI: 10.1016/j.ijbiomac.2022.07.140.

[20] J. S. Bergström and D. Hayman. "An overview of mechanical properties and material modeling of polylactide (PLA) for medical applications". *Annals of biomedical engineering* 44 (2016), 330–340. DOI: 10.1007/s10439-015-1455-8.

[21] K. Cho et al. "Rheological and mechanical properties in polyethylene blends". *Polymer engineering and science* 38 (1998), 1969–1975. DOI: 10.1002/pen.10366.

[22] G. Kalay et al. "Enhancement of the mechanical properties of a high-density polyethylene". *Journal of applied polymer science* 73 (1999), 2473–2483. DOI: 10.1002/(SICI)1097-4628(19990919)73:12<2473::AID-APP16>3.0.CO;2-O.

[23] L. S. Nair and C. T. Laurencin. "Biodegradable polymers as biomaterials". *Progress in polymer science* 32 (2007), 762–798. DOI: 10.1016/j.progpolymsci.2007.05.017.

[24] Q. T. H. Shubhra, A. K. M. Moshiul Alam, and M. A. Quaiyyum. "Mechanical properties of polypropylene composites: A review". *Journal of thermoplastic composite materials* 26 (2013), 362–391. DOI: 10.1177/0892705711428659.

[25] A. Toda. "Spherulitic growth in crystalline polymers". *Encyclopedia of polymers and composites* (2013), 1–12. DOI: 10.1007/978-3-642-37179-0_24-1.

[26] V. Kholodovych and W. J. Welsh. "Densities of amorphous and crystalline polymers". *Physical properties of polymers handbook* (2007), 611–617. DOI: 10.1007/978-0-387-69002-5_37.

[27] A. Toda et al. "Branching and higher order structure in banded polyethylene spherulites". *Macromolecules* 41 (2008), 2484–2493. DOI: 10.1021/ma702267e.

[28] E. M. Woo and G. Lugito. "Cracks in polymer spherulites: Phenomenological mechanisms in correlation with ring bands". *Polymers* 8 (2016), 329–354. DOI: 10.3390/polym8090329.

[29] Y. Liao et al. "Effect of porosity and crystallinity on 3D printed PLA properties". *Polymers* 11 (2019), 1487–1501. DOI: 10.3390/polym11091487.

[30] F. Foglia et al. "Isothermal crystallization of PLA: Nucleation density and growth rates of α and α' phases". *Canadian journal of chemical engineering* 98 (2020), 1998–2007. DOI: 10.1002/cjce.23818.

[31] S. Saeidlou et al. "Poly(lactic acid) crystallization". *Progress in polymer science* 37 (2012), 1657–1677. DOI: 10.1016/j.progpolymsci.2012.07.005.

[32] C. Nakafuku and M. Sakoda. “Melting and crystallization of poly(L-lactic acid) and poly(ethylene oxide) binary mixture”. *Polymer journal* 25 (1993), 909–917. DOI: 10.1295/polymj.25.909.

[33] L. Cartier et al. “Epitaxial crystallization and crystalline polymorphism of polylactides”. *Polymer* 41 (2000), 8909–8919. DOI: 10.1016/S0032-3861(00)00234-2.

[34] Q. Shi et al. “Physical stability of amorphous pharmaceutical solids: Nucleation, crystal growth, phase separation and effects of the polymers”. *International journal of pharmaceutics* 590 (2020), 119925. DOI: 10.1016/j.ijpharm.2020.119925.

[35] J. R. Espinosa et al. “Heterogeneous versus homogeneous crystal nucleation of hard spheres”. *Soft matter* 15 (2019), 9625–9631. DOI: 10.1039/c9sm01142k.

[36] C. Shasteen and Y. B. Choy. “Controlling degradation rate of poly(lactic acid) for its biomedical applications”. *Biomedical engineering letters* 1 (2011), 163–167. DOI: 10.1007/s13534-011-0025-8.

[37] F. Ebrahimi and H. Ramezani Dana. “Poly(lactic acid) (PLA) polymers: from properties to biomedical applications”. *International journal of polymeric materials and polymeric biomaterials* 71 (2022), 1117–1130. DOI: 10.1080/00914037.2021.1944140.

[38] A. Atala. “Tissue engineering and regenerative medicine: concepts for clinical application”. *Rejuvenation research* 7 (2004), 15–31. DOI: 10.1089/154916804323105053.

[39] Q. Chen, S. Liang, and G. A. Thouas. “Elastomeric biomaterials for tissue engineering”. *Progress in polymer science* 38 (2013), 584–671. DOI: 10.1016/j.progpolymsci.2012.05.003.

[40] J. M. Ameer, A. K. Pr, and N. Kasoju. “Strategies to tune electrospun scaffold porosity for effective cell response in tissue engineering”. *Journal of functional biomaterials* 10 (2019), 30–51. DOI: 10.3390/jfb10030030.

[41] S. Pina et al. “Scaffolding strategies for tissue engineering and regenerative medicine applications”. *Materials* 12 (2019), 1824–1866. DOI: 10.3390/ma12111824.

[42] T. S. Karande, J. L. Ong, and C. M. Agrawal. “Diffusion in musculoskeletal tissue engineering scaffolds: design issues related to porosity, permeability, architecture, and nutrient mixing”. *Annals of biomedical engineering* 32 (2004), 1728–1743. DOI: 10.1007/s10439-004-7825-2.

[43] J. A. Sanz-Herrera and E. Reina-Romo. "Cell-biomaterial mechanical interaction in the framework of tissue engineering: insights, computational modeling and perspectives". *International journal of molecular sciences* 12 (2011), 8217–8244. DOI: 10.3390/ijms12118217.

[44] M. N. Collins et al. "Scaffold fabrication technologies and structure/function properties in bone tissue engineering". *Advanced functional materials* 31 (2021), 2010609. DOI: 10.1002/adfm.202010609.

[45] K. Sungsanit, N. Kao, and S. N. Bhattacharya. "Properties of linear poly(lactic acid)/polyethylene glycol blends". *Polymer engineering and science* 52 (2012), 108–116. DOI: 10.1002/pen.22052.

[46] A. Lucke et al. "Biodegradable poly(D, L-lactic acid)-poly(ethylene glycol)-monomethyl ether diblock copolymers: structures and surface properties relevant to their use as biomaterials". *Biomaterials* 21 (2000), 2361–2370. DOI: 10.1016/S0142-9612(00)00103-4.

[47] B. W. Chieng et al. "Poly(lactic acid)/poly(ethylene glycol) polymer nanocomposites: Effects of graphene nanoplatelets". *Polymers* 6 (2014), 93–104. DOI: 10.3390/polym6010093.

[48] A. A. D'souza and R. Shegokar. "Polyethylene glycol (PEG): a versatile polymer for pharmaceutical applications". *Expert opinion on drug delivery* 13 (2016), 1257–1275. DOI: 10.1080/17425247.2016.1182485.

[49] D. Q. M. Craig. "A review of thermal methods used for the analysis of the crystal form, solution thermodynamics and glass transition behaviour of polyethylene glycols". *Thermochimica acta* 248 (1995), 189–203. DOI: 10.1016/0040-6031(94)01886-L.

[50] M. Goffin. "Development of porous biodegradable polymer materials for biological applications". MA thesis. Louvain-la-Neuve: UCLouvain, 2022.

[51] X.-F. Wei et al. "Greatly accelerated crystallization of poly(lactic acid): cooperative effect of stereocomplex crystallites and polyethylene glycol". *Colloid and polymer science* 292 (2014), 163–172. DOI: 10.1007/s00396-013-3067-x.

[52] H. Younes and D. Cohn. "Phase separation in poly(ethylene glycol)/poly(lactic acid) blends". *European polymer journal* 24 (1988), 765–773. DOI: doi.org/10.1016/0014-3057(88)90013-4.

[53] I.-G. I. Athanasoulia et al. "The effect of poly(ethylene glycol) mixed with poly(L-lactic acid) on the crystallization characteristics and properties of their blends". *Polymer international* 68 (2019), 788–804. DOI: 10.1002/pi.5769.

[54] H. D. Keith and F. J. Jr. Padden. “A phenomenological theory of spherulitic crystallization”. *Journal of applied physics* 34 (1963), 2409–2421. DOI: 10.1063/1.1702757.

[55] A. S. Altorbaq et al. “Crystallization kinetics and nanoparticle ordering in semicrystalline polymer nanocomposites”. *Progress in polymer science* (2022), 101527. DOI: 10.1016/j.progpolymsci.2022.101527.

[56] I. Pillin, N. Montrelay, and Y. Grohens. “Thermo-mechanical characterization of plasticized PLA: Is the miscibility the only significant factor?” *Polymer* 47 (2006), 4676–4682. DOI: 10.1016/j.polymer.2006.04.013.

[57] C. Courgneau et al. “Analysis of the structure-properties relationships of different multiphase systems based on plasticized poly(lactic acid)”. *Journal of polymers and the environment* 19 (2011), 362–371. DOI: 10.1007/s10924-011-0285-5.

[58] C. Park et al. “Effect of hydrophilicity on the biodegradability of polyesteramides”. *Journal of applied polymer science* 90 (2003), 2708–2714. DOI: 10.1002/app.12925.

[59] F. J. Li et al. “Tensile properties of polylactide/poly(ethylene glycol) blends”. *Journal of polymers and the environment* 23 (2015), 407–415. DOI: 10.1007/s10924-015-0718-7.

[60] P. Saini, M. Arora, and M. N. V. R. Kumar. “Poly(lactic acid) blends in biomedical applications”. *Advanced drug delivery reviews* 107 (2016), 47–59. DOI: 10.1016/j.addr.2016.06.014.

[61] N. Annabi et al. “Controlling the porosity and microarchitecture of hydrogels for tissue engineering”. *Tissue engineering part B: Reviews* 16 (2010), 371–383. DOI: 10.1089/ten.teb.2009.0639.

[62] F. Dehghani and N. Annabi. “Engineering porous scaffolds using gas-based techniques”. *Current opinion in biotechnology* 22 (2011), 661–666. DOI: 10.1016/j.copbio.2011.04.005.

[63] A. Thorvaldsson et al. “Electrospinning of highly porous scaffolds for cartilage regeneration”. *Biomacromolecules* 9 (2008), 1044–1049. DOI: 10.1021/bm701225a.

[64] A.-V. Do et al. “3D printing of scaffolds for tissue regeneration applications”. *Advanced healthcare materials* 4 (2015), 1742–1762. DOI: 10.1002/adhm.201500168.

[65] M. J.-C. Nalbandian. “Development and optimization of chemically-active electrospun nanofibers for treatment of impaired water sources”. PhD thesis. Riverside: University of California, 2014.

[66] C. W. Li and G. J. Wang. "MEMS manufacturing techniques for tissue scaffolding devices". In: *MEMS for Biomedical Applications*. Cambridge: Elsevier, 2012, 192–217. DOI: 10.1533/9780857096272.3.192.

[67] H.-J. Chung and T.-G. Park. "Surface engineered and drug releasing prefabricated scaffolds for tissue engineering." *Advanced drug delivery reviews* 59 4-5 (2007), 249–62. DOI: 10.1016/j.addr.2007.03.015.

[68] G. I. J. Salentijn et al. "Fused deposition modeling 3D printing for (bio)analytical device fabrication: procedures, materials, and applications". *Analytical chemistry* 89 (2017), 7053–7061. DOI: 10.1021/acs.analchem.7b00828.

[69] Z. Liu et al. "A critical review of fused deposition modeling 3D printing technology in manufacturing polylactic acid parts". *The international journal of advanced manufacturing technology* 102 (2019), 2877–2889. DOI: 10.1007/s00170-019-03332-x.

[70] D. Rigon, M. Ricotta, and G. Meneghetti. "A literature survey on structural integrity of 3D printed virgin and recycled ABS and PP compounds". *Procedia structural integrity* 28 (2020), 1655–1663. DOI: 10.1016/j.prostr.2020.10.139.

[71] I. Buj-Corral et al. "Characterization of 3D printed metal-PLA composite scaffolds for biomedical applications". *Polymers* 14 (2022), 2754–2766. DOI: 10.3390/polym14132754.

[72] N. Rodrigues et al. "Manufacture and characterisation of porous PLA scaffolds". *Procedia cirp* 49 (2016), 33–38. DOI: 10.1016/j.procir.2015.07.025.

[73] R. Baptista and M. Guedes. "Morphological and mechanical characterization of 3D printed PLA scaffolds with controlled porosity for trabecular bone tissue replacement". *Materials science and engineering: C* 118 (2021), 111528. DOI: 10.1016/j.msec.2020.111528.

[74] H. M. Yin et al. "Engineering porous poly(lactic acid) scaffolds with high mechanical performance via a solid state extrusion/porogen leaching approach". *Polymers* 8 (2016), 213–226. DOI: 10.3390/polym8060213.

[75] Q. Ren et al. "Fabrication of super-hydrophilic and highly open-porous poly(lactic acid) scaffolds using supercritical carbon dioxide foaming". *International journal of biological macromolecules* 205 (2022), 740–748. DOI: 10.1016/j.ijbiomac.2022.03.107.

[76] S. J. Hollister. "Porous scaffold design for tissue engineering". *Nature materials* 4 (2005), 518–524. DOI: 10.1038/nmat1421.

[77] K. Akhtar et al. “Scanning electron microscopy: Principle and applications in nanomaterials characterization”. *Handbook of materials characterization* (2018), 113–145. DOI: 10.1007/978-3-319-92955-2_4.

[78] J. Gao, P. M. Crapo, and Y. Wang. “Macroporous elastomeric scaffolds with extensive micropores for soft tissue engineering”. *Tissue engineering* 12 (2006), 917–925. DOI: 10.1089/ten.2006.12.917.

[79] M. Kuterbekov et al. “Solvent-free preparation of porous poly(L-lactide) microcarriers for cell culture”. *Acta biomaterialia* 75 (2018), 300–311. DOI: 10.1016/j.actbio.2018.06.009.

UNIVERSITÉ CATHOLIQUE DE LOUVAIN
École polytechnique de Louvain
Rue Archimède, 1 bte L6.11.01, 1348 Louvain-la-Neuve, Belgique | **www.uclouvain.be/epl**